Doctoral Dissertation (Censored)
博士論文（要約）

Australasian Tektite Event: Identification of the On-land Ejecta Deposit and its Distribution across Eastern Indochina

（オーストラリア・アジアテクタイトイベント：
インドシナ半島東部における陸上イジェクタ層の認定と
その分布）

A Dissertation Submitted for the Degree of Doctor of Philosophy
December 2020

令和 2 年 12 月博士（理学）申請

Department of Earth and Planetary Science,
Graduate School of Science, The University of Tokyo
東京大学大学院理学系研究科地球惑星科学専攻

Toshihiro Tada
多田賢弘

Abstract

The Australasian Tektite Event (AATE) occurred ca. 0.8 Ma is the youngest record of a large impact event on the Earth. Based on the wide distribution of the tektite—from Southeast Asia to Antarctica—the magnitude of the impact has been estimated as large enough to create a 30–120 km sized crater. Although it has been estimated that the impact occurred somewhere in eastern Indochina, the crater has never been located definitively despite intensive search efforts, and the nature of the impact, such as the location, magnitude, and target rocks, are not well constrained.

In general, the distribution and composition of the proximal ejecta deposits have information about the location, magnitude, and target rock of the impact. Especially, the distribution of the thickness of an ejecta deposit is important to constrain the location of the impact since the thickness of an ejecta deposit increases toward the impact location. As for the AATE, however, the ejecta deposit proximal to the estimated impact area in eastern Indochina has never been identified.

There are several reports of tektites found within a stratum called the "laterite" layer that is widely distributed in eastern Indochina. It has long been debated whether these tektites are in situ or reworked. This uncertainty is due to the lack of detailed description of the field occurrence of the tektites and tektite-bearing Quaternary deposits, and the lack of evidence of shock metamorphism (such as shocked minerals) other than the tektites in Indochina.

To identify the proximal ejecta deposit in eastern Indochina and clarify its lithostratigraphy, distribution, and depositional process for a better understanding of the nature of the AATE, field surveys of the Quaternary deposits were conducted at 20 sites across eastern Indochina (northeastern Thailand, Southern Laos, northern Cambodia, and central Vietnam).

The detailed occurrence of tektite fragments found within the "laterite" layer at the HO06 section in Ubon Ratchathani province, northeastern Thailand, was described demonstrating the evidence of the in-situ occurrence of these tektite fragments. At least 331 tektite fragments with a total weight of 713 g were found from a 40 x 30 cm area with 10 cm thickness in the upper part of the "laterite" layer. The very angular shapes and very poorly-sorted nature of the tektite fragments, the similar chemical composition of the fragments, and the restoration of larger tektite fragments into one ellipsoidal tektite mass

suggest that these tektite fragments were formed by fragmentation of one large tektite mass. The fact that the fragments were found within the "laterite" layer is inconsistent with the previous interpretation that the upper surface of the "laterite" layer is a paleo-erosional surface, on which the tektites were reworked. The fragments' size distribution is bifractal following two power laws in the range from 10 to 26 mm and 26 to 37 mm, with fractal dimensions (Ds) of 2.2 and 7.5, respectively. The Ds for the coarse fraction of the tektite fragments is larger than the Ds for rock fragments generated by rockfalls and rock avalanches and similar to the Ds for the coarser fraction fragments generated by high-speed impact experiments. This large Ds value suggests that the tektite fragments were formed through intense fragmentation by a relatively high energetic process. The occurrence of the fragments forming a cluster and the distribution of the fragments in sediments revealed by a computer tomography scanning analysis indicate that the fragments were not moved apart significantly after fragmentation and burial. Based on these results, it is concluded that the mass of a tektite was fragmented at the time of the landing on the ground after the ejection from the impact site and has not been disturbed further (i.e., in situ).

In addition to the in-situ occurrence of the tektite fragments, I reported the discovery and occurrence of shocked quartz with planar deformation features (PDFs) from the Quaternary depositional sequence, including the "laterite" layer, at the Huai Om section in Ubon Ratchathani province, northeastern Thailand. Measurements of the orientation of lamellae with a universal stage microscope and observation using scanning electron microscopy and transmission electron microscopy were conducted to confirm the presence of PDFs.

The extensive field survey at 20 sites (including the Huai Om and HO06 sections) across a wide area in eastern Indochina revealed that there are basically the same lithostratigraphic units (Units 1-3 in ascending order) unconformably covering the basement rocks and sediments.

Unit 1 is composed of gravely silt to sand layers or a sandy gravel layer containing materials reworked from the local basement. The thickness of Unit 1 is about 30 cm to 2 m. This unit is not laterally continuous and absent at several localities. Unit 2 is composed of a very poorly sorted breccia corresponding to the "laterite" layer. The thickness of Unit 2 is about 30 cm to more than 9 m. Tektites were found at several sites at the top of or within the upper part of this unit. Unit 3 is composed of a well-sorted silt to fine sand

layer. Although the original thickness of this unit is unknown because this unit is truncated and capped by modern soil, the observed thickness of Unit 3 varies from site to site, about 30 cm to 3 m.

Based on the in-situ occurrence of tektites in Unit 2 at HO06 section, the discovery of shocked quartz grains throughout Units 1-3 at Huai Om section, and continuous distribution of Units 2-3 in a wide area, the ejecta-bearing sequence of this region (Units 1-3) was identified as the proximal ejecta deposit of the AATE.

Based on their stratigraphy and lithological and sedimentological evidence, Units 1-3 are considered as deposited by the following process: rework of the local basement rocks by the impact-generated wind loaded with fine ejecta (Unit 1), followed by deposition of the ejecta curtain materials including gravels and tektites (Unit 2), and finally deposition of fallout fine ejecta (Unit 3).

The thickness of Unit 2 becomes thicker toward southwestern Laos. This thickness distribution of Unit 2, as well as the fact that the size of gravels in Unit 2 becomes larger toward southwestern Laos, indicates that the location of the impact is somewhere in southwestern Laos. The regression analysis of the distribution of the thickness of Unit 2, assuming that the log thickness is negatively correlated with log distance from a source area, indicates that the Bolaven Plateau area (15.2°N, 106.1°E) is the most probable impact site of the AATE. The presence of the weathered basalt fragments, sandstone and mudstone fragments, and fragments of rounded quartzite gravels in Unit 2 indicates that the target rock of the AATE includes basalt, Mesozoic sedimentary basement rocks, and possibly Quaternary river gravels. This estimation of the target rocks is consistent with the estimation of the impact site in southwestern Laos, where Neogene to Quaternary basalt lava and Mesozoic sedimentary rocks are widely distributed. The result of the estimation of the impact site strongly supports the hypothesis of Sieh et al. (2019) that the AATE occurred in the basalt field of the Bolaven Plateau, and the crater was buried by younger basalts that erupted after the impact.

Contents

Chapter 1
General Introduction

1.1. The problems in the studies on the Australasian tektite event

Hypervelocity impacts by large extra-terrestrial objects can cause catastrophic influence on the Earth's surface environment and ecosystem, as is the case of the Chicxulub (K/Pg) impact at the end of the Cretaceous period (Alvaletz et al. 1980; Pierazzo and Artemieva 2012; Schulte et al. 2010). Despite 200 impact craters found on the Earth so far (Schmieder and Kring 2020), previous studies on large impact events have been conducted mostly on a few impact events, such as the K/Pg boundary event. Studying impact events on the Earth is generally difficult since weathering, erosion, sedimentation, and tectonic movements have erased the geological evidence of impacts, such as craters and proximal ejecta deposits. Evidence of impacts and environmental perturbations is more likely preserved for younger impacts. It is, therefore, essential to study young and large impact events.

The Australasian Tektite Event (AATE), which occurred at ca. 0.8 Ma (it is estimated to be 788.1±3.0 ka by Jourdan et al. (2019), 793±14 ka by Schwarz et al. (2016), 800±6 ka by Yamei et al. (2000)), should be important to study impact phenomena because it is the youngest among known large impact events on the Earth. Tektites are glass objects formed by melting of crustal rocks due to impacts (e.g., Koeberl 1994). They are distributed in at least four broad areas of the Earth's surface, called strewn fields (e.g., Koeberl 1994; Glass and Simonson 2012). The Australasian tektite strewn field is the youngest and largest strewn field extending from southwestern China, through Indochina, Australia, to Antarctica (Fig.1.1A) (e.g., Folco et al. 2016).

The possible effects of AATE on the regional environment and ecosystem has been suggested. It is implied that AATE has relevance to the penecontemporaneous (~0.8 Ma) large flood deposits in northeastern Thailand, which includes tektites, carbonized wood trunks, and bones of large mammals (Haines et al. 2004). The effects of AATE on early hominid dispersion and settlement have also been suggested (e.g., Hyodo et al. 2011; Li et al. 2020). The early hominid migrated into Southeast Asia by 1.3 Ma at the latest (Matsu'ura et al. 2020). Thus, hominids settled in Southeast Asia must have suffered catastrophic effects from the impact. The population reduction due to the impact was

implied by the stratigraphic coincidence of the last occurrence of hominid fossils and tektite-bearing horizon in Sangiran area, Java (Hyodo et al. 2011), and the sparse distribution of stone tools, which buried in the same layer with Australasian tektites, at Bose, southern China (Yamei et al. 2000; Li et al. 2020).

Despite the large size and young age of the strewn field and the possible effects on the regional environment and ecosystem in Southeast Asia, the source crater and proximal ejecta deposit of AATE have never been conclusively identified. Thus, the nature of the impact, such as the location, magnitude, impact angle and direction, and types of the target rock, is not well understood.

Based on several lines of evidence, the location of the impact is presumed somewhere in the eastern part of the Indochina Peninsula (Fig.1.1B) (Schnetzler, 1992; Ma et al. 2004; Glass and Koeberl 2006; Prasad et al. 2007; Sieh et al. 2019). The limited distribution of the Muong Nong-type (layered) tektites, which are considered to be proximal to the impact site based on their large size, blocky shape, internal heterogeneous texture, and high volatile content (Koeberl 1992; Cavosie et al. 2018), suggests that the crater is in the area around northeastern Thailand and southwestern Laos (Schnetzler 1992). Ma et al. (2004) suggested that the crater is in a coastal region of central Vietnam based on geographical variation of ^{10}Be concentrations in tektites from a broad area of Southeast Asia. The geographical distribution of microtektites in marine sediment cores suggested that the crater is in the northeastern part of the Indochina Peninsula (e.g., Glass and Koeberl 2006; Prasad et al. 2007). Recently, Sieh et al. (2019) proposed that the impact occurred on the basalt field of the Bolaven Plateau in southwestern Laos, and the crater was buried by younger basalt erupted after the impact, based on the presence of a basalt component in the geochemistry of the tektites, pre- and postimpact ages of the basalt, negative gravity anomaly in the basalt field, and the presence of a possible ejecta deposit in southern Laos.

The magnitude of the impact has been roughly estimated as large enough to create a 30–120 km sized crater based on the distribution of the thickness of the microtektite layer in marine sediment cores (Glass and Koeberl 2006; Glass and Pizzuto 1994; Lee and Wei 2000; Prasad et al. 2007). The asymmetric shape of the Australasian tektite strewnfield, similar to the "Butterfly" pattern of ejecta distribution known to be formed by oblique impacts, implies that the AATE was an oblique impact from the northwest (Fig. 1.1A) (e.g., Ford 1988). However, the shape of the Australasian tektite strewn field

relies on the distribution of the microtektites, which is not established yet, and there is a possibility that the strewn field extends further (Tada et al. 2020; Schwarz et al. 2016).

The information on the target rocks of AATE has been provided by the geochemistry of the tektites since the target rock of the impact is the source material from which tektites were formed. The major and trace element composition of Australasian tektites suggests that the source material of the Australasian tektites is post-Archean upper continental crust materials, presumably sediments. (e.g., Koeberl 1990, 1994; Mizera et al. 2016). Koeberl (1992) interpreted the major element composition of Muon Nong-type Australasian tektites as a mixture of soils from Thailand and Cambodia, quartzite, and loess from southern China. On the other hand, Sieh et al. (2019) conducted the principal component analysis of the major element composition of the Australasian tektites and demonstrated that the major element composition can be interpreted as a mixture of basalt and regionally distributed Mesozoic quartz-rich sandstone. However, basalts do not seem suitable for the source material of Australasian tektites based on the rare earth-element pattern of the Australasian tektites similar to the upper continental crust (Koeberl 1992). The high concentration of ^{10}Be in the Australasian tektites shows that the source material includes surface or near-surface sedimentary deposits (Ma et al. 2004). The Nd and Sr isotope study provides a constraint on the source material as a sedimentary formation of Jurassic age, i.e., 175 ± 15 Ma (Blum et al. 1992).

Species of the relict minerals found in the Australasian tektite (zircon, rutile, chromite, quartz), their rounded shape, and good sorting also indicate that the source material is silt to fine-sand sedimentary material (Glass and Barlow 1979). Unmelted and partly melted ejecta grains found in the South China Sea microtektite layer also suggest that silt to fine sand sedimentary material were included as the target rock of the impact (Glass and Koeberl 2006).

The uncertainty on the location, magnitude, impact angle, impact direction, and types of target rocks described above is derived from the lack of information on proximal ejecta deposits on-land in the Indochina Peninsula. In general, the thickness of ejecta deposits varies with distances from the crater and magnitude of the impact (e.g., Mcgetchin et al. 1973), and thus, the distribution of the proximal ejecta deposits has information of the location and magnitude of the impact. An oblique impact with an angle of less than 30 degrees causes asymmetric distribution of ejecta deposits (e.g., Melosh 1989). The asymmetric distribution of ejecta also has information on the direction of the

oblique impact. In addition, gravels in ejecta deposits provide direct information on the target rocks of the impact. Thus, to better understand the nature of the AATE, the ejecta deposit and its distribution around the estimated impact area are important. Although the distal ejecta layer of the AATE has been recognized as the microtektite layer in marine sediment cores at multiple locations (e.g., Prasad et al. 2007), the proximal ejecta layer of the AATE has never been identified on land in Indochina Peninsula.

There are several sites in Indochina Peninsula where tektites have been reported from the Quaternary depositional sequence (Barnes and Pitakpaivan 1962; Tamura 1992; Wasson et al. 1995; Schnetzler and McHone 1996; Fiske et al. 1996, 1999; Songtham et al. 2011, 2012). In these cases, tektites are found from the upper part of or at the top of a so-called "laterite layer", which is a loose nodular reddish-black ferruginous layer broadly distributed a few meters below the surface in Southeast Asia (e.g., Tamura 1992; Fiske et al. 1996; Songtham et al. 2011, 2012) (the occurrence of the tektites previously reported in Southeast Asia are summarized in detail in section **2.1.1**). It has been considered that the tektites in the "laterite" layer were directly deposited in the strata and hence considered as in situ by several authors (Wongsomsak 1986; Tamura 1992; Songtham et al. 2011, 2012; Nuchanong et al. 2014). On the other hand, the possibility of reworking of tektites after the impact has been claimed (Fiske et al. 1996; Keates 2000; Koeberl and Glass 2000; Langbroek 2015) due to the lack of detailed sedimentological description of tektites and tektite-bearing deposits and the lack of other evidence of impact such as shock deformed minerals. Sieh et al. (2019) reported that the bouldery breccia in southern Laos may be a probable ejecta deposit based on the findings of quartz grains with apparent planar features that they believe to be planar deformation features (PDFs), a diagnostic feature to identify shocked quartz (e.g., Chao 1967; French and Koeberl 2010). However, Sieh et al. (2019) did not conduct comprehensive identification of PDFs, which is usually required for identification of shocked quartz, as discussed in detail in section **3.1.2**.

1.2. Geological setting of the study area

The study sites cover a wide area across eastern Indochina, including northeastern Thailand, southern Laos, central Vietnam, and northern Cambodia. In this section, I summarize the geological setting of the basement rocks and descriptions of the Quaternary sedimentary sequence in the study area by the previous studies.

Eastern Indochina is characterized by a large sedimentary basin called the Khorat Plateau Basin (Minezaki et al. 2019), extending over 200, 000 km^2 and covering northeastern Thailand, western Laos, and northern Cambodia (Fig. 1.2A). The Khorat Plateau Basin is composed of a complex sequence of five basins filled during five periods of deposition from the Late Carboniferous to the end of the Cretaceous, which are separated by unconformities formed by the Indosinian orogenic events initiated by the collision between South China and Indochina blocks during Late Permian to Early Triassic (Booth and Sattayarak, 2011; Minezaki et al. 2019). The Khorat Group, which is thick (2000-3000 m) non-marine sedimentary rocks, overlies the Indosinian Ⅲ unconformity corresponding to the orogenic event in Early Jurassic, and extends to the mid-Cretaceous unconformity. The Khorat Group is composed of conglomerates, sandstones, and mudstones (Racey et al. 1996; Booth and Sattayarak 2011; Minezaki et al. 2019). The Maha Sarakham Formation composed of mid-Cretaceous evaporites and siliciclastic mudstone and the Phu Tok Formation composed of Late Cretaceous aeolian sandstone locally overlie the Khorat Group with the mid-Cretaceous unconformity (e.g., Racey 1996; Hasegawa et al. 2010).

In the study area, Neogene to Quaternary basalts are distributed mainly in the area of the Bolavean Plateau in southwestern Laos (Vilayhack et al. 2008; Negishi et al. 2009; Sieh et al. 2019) and locally in the southern margin of northeastern Thailand, and northern Cambodia (e.g., Fedorov & Koloskov 2005) (Fig. 1.2B). The age of the basalt in the Bolaven Plateau was dated as 16 Ma to 27 Ka by Ar-Ar dating (Sieh et al. 2019).

The Quaternary deposits unconformably overlie the Mesozoic sedimentary basement and well described only in northeastern Thailand. The typical thickness of the Quaternary deposits in the Khorat Plateau Basin, along the main rivers (the Mun, Chi, and the Mekong rivers), is 35 to 80 m (Nuchanong et al., 2014). The Quaternary deposits are composed of gravel beds that are considered as river terrace deposits (Tamura et al. 1992; Nuchanong et al., 2014), at the base, which is overlain by the "laterite" layer including tektites and then by the silt to fine sand layer in ascending order (Songtham et al. 2011, 2012). Away from the main rivers, the Quaternary deposits are devoid of river terrace deposits, and the "laterite" layer lies directly on the Mesozoic sedimentary basement. The thickness of the "laterite" layer plus the overlying silt to sand layer is several meters (Fiske et al. 1996; Tamura 1992). The clasts in the gravel beds are mainly well-rounded quartzite, and rounded and platy sandstone with a minor amount of flint and

chert. These clasts are considered as derived from the conglomerates of the Mesozoic sedimentary basement (Tamura 1992; Choowing 2011).

The overlying silt to sand layer, known as "Yasothon soil" or "Cover-sand", is quartz-rich massive silt to sand widely distributed through southern China, Laos, Vietnam, northern Cambodia, and northeastern Thailand (Tamura 1992; Demeter et al. 2010; Nichol and Nichol 2015). The "Yasothon soil" has been considered to be a loess deposit formed under arid climate based on the homogeneous and well-sorted texture, and sub-spherical sub-rounded grain shape (Tamura, 1992; Nichol and Nichol, 2015). Sanderson et al. (2001) reported a luminescence date of younger than 40 ka for a fine sand layer directly beneath the ground surface at one site in Khon Kaen district in northeastern Thailand. Nichol and Nichol (2015) use this luminescence date as supporting evidence for the hypothesis that the fine sand layer is loess, deposited during the last glacial period.

On the other hand, Bunopus et al. (1999) and Songtham et al. (2011, 2012) proposed that the "Yasothon soil" is widely distributed fine ejecta derived from the AATE, but they did not show any conclusive evidence of impact origin, such as an occurrence of shock-metamorphosed minerals.

1.3. The purpose and the structure of this thesis

This thesis aims to identify the on-land ejecta deposit in the Indochina Peninsula and to clarify its lithostratigraphy, distribution, and depositional process for a better understanding of the nature of the AATE.

Chapter **2** of this thesis reports a detailed occurrence of tektite fragments found within the "laterite" layer at a section designated HO06 in Ubon Ratchathani province, northeastern Thailand, to investigate whether the tektite fragments of similar occurrence are of primary depositional origin or reworked origin deposited after the impact event. The very angular shapes and very poor sorting of the tektite fragments, similar chemical composition of the tektite fragments, restoration of a part of the original MN tektite mass, and the CT scan analysis revealed that the tektite fragments were formed by fragmentation of one large tektite mass at the time of the landing after the ejection by the impact, and has not been disturbed further (i.e., in situ).

Chapter **3** of this thesis reports detailed lithostratigraphy of the Quaternary sequence, including the "laterite layer" and discovery of the shocked quartz grains with

planar deformation features (PDFs) throughout the sequence at Huai Om section in Ubon Ratchathani province, northeastern Thailand. The Quaternary sequence in this region can be divided into three lithostratigraphic units (Units 1-3 in ascending order). Shocked quartz grains with PDFs were found through the Units 1-3. PDFs were identified by observation under an optical microscope, measurement of their orientation with a universal stage microscope, and SEM and TEM observations.

Chapter **4** of this thesis reports the field survey results across eastern Indochina (northeastern Thailand, southern Laos, northern Cambodia, and central Vietnam) to investigate the distribution of the ejecta bearing sequence (Units 1-3) described in Chapters **2** and **3**. The result revealed that the tektite-bearing gravel layer (Unit 2) and the overlying silt to fine sand layer (Unit 3) are continuously distributed in a wide area in eastern Indochina.

In Chapter **5** of this thesis, the ejecta-bearing sequence (Units 1-3) of this region is identified as the proximal ejecta deposit of the AATE based on the in-situ occurrence of tektites in the upper part of Unit 2 (Chapter **2**), the discovery of shocked quartz grains throughout Units 1-3 (Chapter **3**) and continuous distribution of Units 2-3 over a wide area (Chapter **4**). The depositional processes of Units 1-3 and implications for the location, magnitude, and target rocks of AATE are discussed based on the lithostratigraphy, distribution of thickness and grain size, and types of gravels in the ejecta deposit.

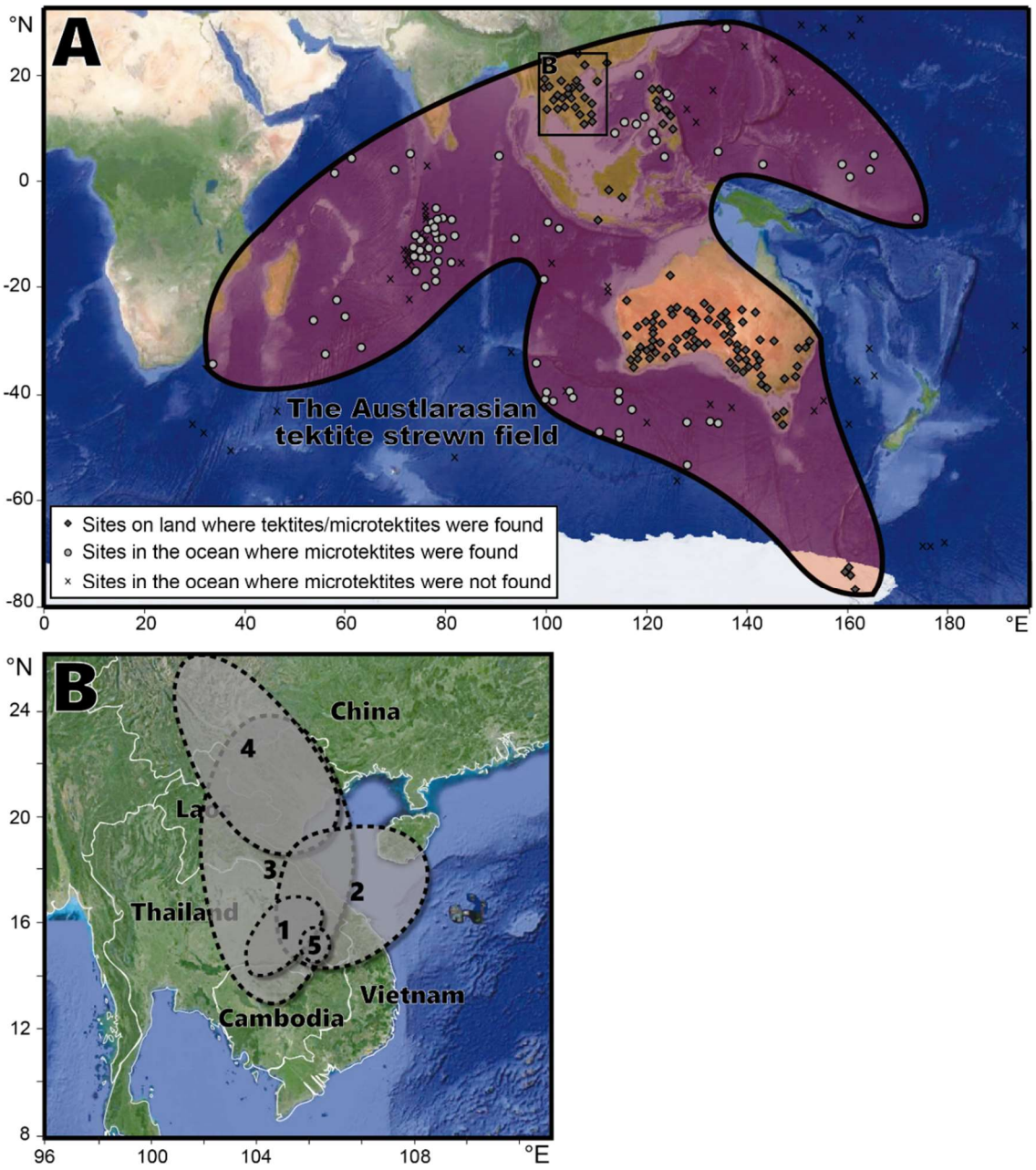

Figure 1.1 A) Distribution of the Australasian Tektites. The solid line indicates the boundary of the strewn field defined by the occurrence of the microtektites in marine sediment cores and on Antarctica (after Folco et al. 2011). The sites where tektites are found on land are after Folco et al. (2011) and Glass and Koeberl (2006). B) Estimated areas for the location of the AATE. (1) Schnetzler 1992, (2) Ma et al. 2004, (3) Glass and Koeberl 2006, (4) Prasad et al. 2007, (5) Sieh et al. 2019.

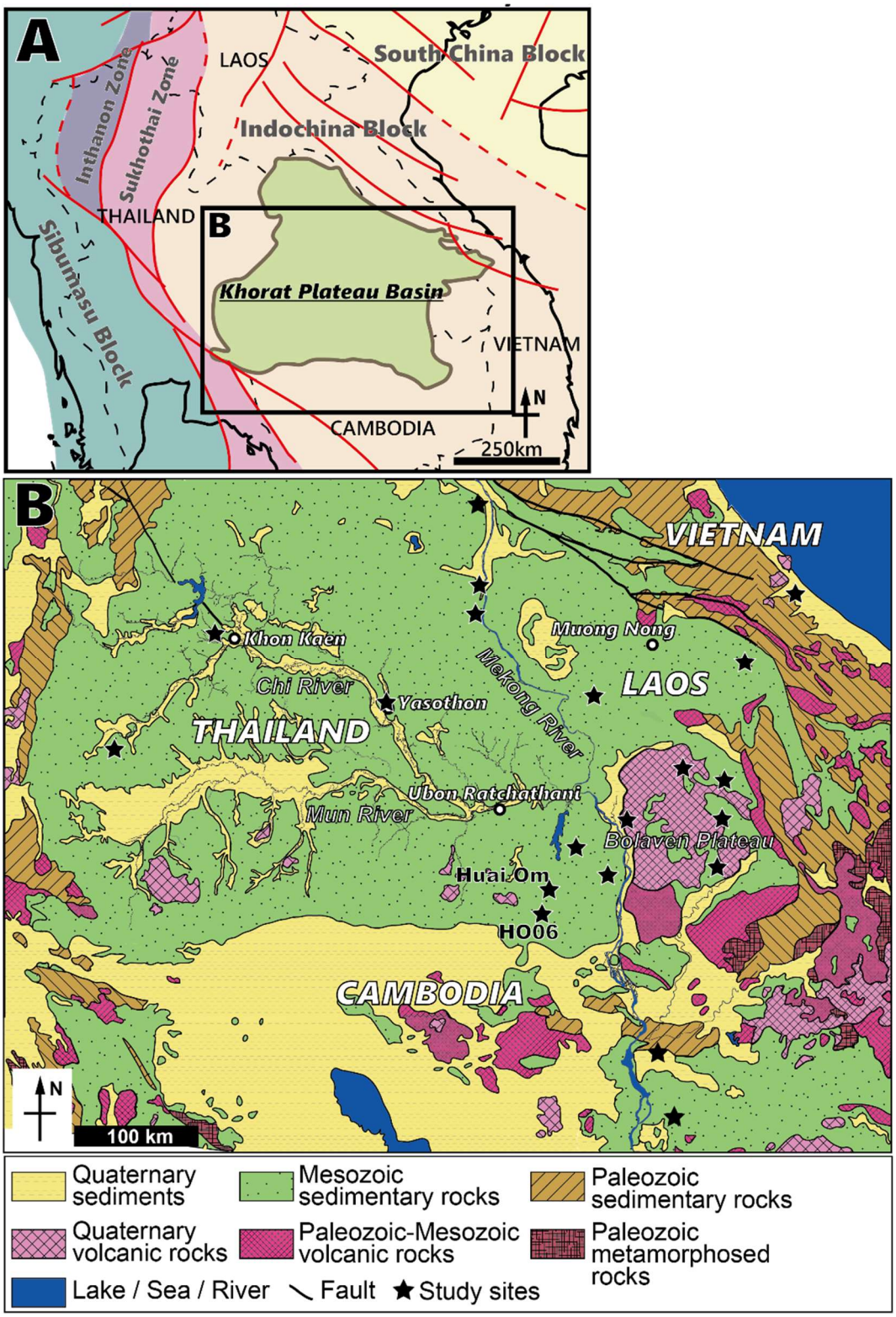

Figure 1.2 A) Location of the Khorat Plateau Basin and major tectonic subdivisions of Indochina (modified from Minezaki et al. 2019). B) Geological map of the study area (modified after Teraoka and Okumura 2011). Locality names mentioned in Chapter 1 are also shown.

Chapter 2

In-situ Occurrence of Muong Nong-type Tektite Fragments at HO06 Section, Northeastern Thailand

2.1 Introduction

2.1.1 Previous studies on the occurrence of Australasian tektites on land in the Indochina Peninsula

Australasian tektites found on land have been classified into three groups based on their morphology (e.g., Koeberl 1994): (1) splash-form (also called as normal type), (2) ablated form (also called as aerodynamically shaped), and (3) Muong Nong-type (MN) tektites (also called as layered tektites). Splash form tektites are reported from a wide area of Southeast Asia. They are generally several cm in size and have symmetrical shapes such as spheres, droplets, teardrops, and dumbbells. These shapes of the splash form tektites are considered to be resulted from the solidification of rotating liquids during their flight after ejection from the impact point (Stauffer and Butler 2010). Abrated tektites are reported from Australia. They are several cm in size and have shapes like a flanged button. The shapes of the abrated tektites are resulted from partial re-melting during atmospheric re-entry after they were ejected outside the atmosphere (e.g., McCall 2001).

MN tektites are distributed in limited areas across northeastern Thailand, southern Laos, Cambodia, Vietnam, and Hainan Island in China (Fig. 2.1) (Schnetzler 1992; Wasson et al. 1995; Schnetzler and McHone 1996; Lin and Uda 1997; Fiske et al. 1999; Shimo et al. 2010). They are typically > 10 cm, and the largest MN tektite reported so far is 24.1 kg in weight (Koeberl 1992). They have blocky shapes and internal layered textures. Based on their large size, blocky shape, internal heterogeneous texture, and high volatile content, MN tektites are considered proximal to the impact site (Koeberl 1992; Cavosie et al. 2018).

Although there are many studies on microstructure and geochemistry of Australasian tektites, most of them were conducted on samples of uncertain or unknown provenance (e.g., Fudali et al. 1987; Wasson 1991; Schnetzler and McHone 1996; Herzog et al. 2008). Although most Australasian tektites reported with their provenances were found as rubbles left on the ground surface, there are several reports of tektites found

from the Quaternary deposits of Indochina Peninsula (Fig. 2.1), of which occurrences are summarized in Table 2.1 (Barnes and Pitakpaivan 1962; Tamura 1992; Wasson et al. 1995; Fiske et al. 1996, 1999; Schnetzler and McHone 1996; Lin and Uda 1997; Shimo et al. 2010; Songtham et al. 2011, 2012). According to these studies, tektites were found from the upper part or at the top of a gravel (granule to pebble-bearing sand) layer containing reddish-black spherical- to irregular-shaped ferruginous nodules, called a "laterite" layer. However, the details of the occurrence of the tektites in the "laterite" layer were not provided.

The tektites recovered from the "laterite" layer have been considered by several authors to have deposited directly in the strata and found in situ (Wongsomsak 1986; Tamura 1992; Songtham et al. 2011, 2012; Nuchanong et al. 2014). On the other hand, there is a claim that these tektites have been reworked, based on the following reasons (Fiske et al. 1996; Keates 2000; Koeberl and Glass 2000; Langbroek 2015).

Fiske et al. (1996) conducted field surveys at two localities in Ubon Ratchathani province, northeastern Thailand (Huai Om and Huai Sai). They found two fragments of MN tektite at the top of the "laterite" layer exposed along a dam spillway at Huai Om. At Huai Sai, they conducted a controlled excavation of a 3 × 3m area and found 1139 MN tektite fragments with a total weight of 6 kg forming a cluster at the top of the "laterite" layer. They concluded that these MN tektite fragments were resulted from the fragmentation of one large tektite mass, based on their occurrence that many fragments form a cluster, the similar chemical composition of the fragments, and the size distribution of the fragments that follows a power law. Based on the hardly cemented appearance of the upper surface of the "laterite" layer that looks like an erosional pavement, they interpreted that the top of the "laterite" layer is a paleo-erosional surface and that the tektite fragments found at the top of the "laterite" layer were reworked on the paleo-erosional surface. However, their interpretation is based only on the hard-cemented appearance of the "laterite" layer in the field. Despite their conclusion that the tektite fragments were reworked, Fiske et al. (1996) also noted that the tektite fragments remain as a cluster and there is no positive evidence that these fragments have undergone significant lateral transport. Thus, their interpretation does not seem to be well supported by their own observations. However, this point has long been overlooked, and their conclusion has been widely accepted.

Australasian tektites reported in Australia generally are in deposits dated as younger than the AATE, and thus, these tektites are interpreted to be reworked (e.g., Fudali 1993). Koeberl and Glass (2000) and Keates (2000) claimed that tektites in the "laterite" layer in the Indochina Peninsula might have also been reworked by analogy with the observation in Australia, although there is no such field evidence from Southeast Asia.

2.1.2 The purpose of this chapter

In this chapter, I aim to clarify whether the Australasian tektites in the "laterite" layer are of primary depositional origin (in situ) or reworked. If these tektites are of primary depositional origin, it is indicated that the "laterite" layer could be a part of the ejecta deposit of AATE. For this purpose, the occurrence of tektite fragments found within the "laterite" layer at a section designated HO06 in Ubon Ratchathani province, northeastern Thailand, was reported in detail. In addition to the detailed description of the field occurrence of the tektite fragments, computer tomography (CT) scanning of a block sample taken from the area where the tektite fragments were found was conducted to describe their occurrence in three dimensions. The major element compositions of nine tektite fragments were analyzed by electron probe microanalysis (EPMA) to demonstrate that they have similar chemical composition. A part of an original tektite mass was restored using large tektite fragments recovered from the block sample to demonstrate that these tektite fragments originally formed one large MN tektite mass. The size distribution analysis of the tektite fragments was further conducted to investigate the fragmentation process of the original tektite mass.

The main part of this chapter was already published as Tada et al. (2020) from Progress in Earth and Planetary Science.

2.2 Study site

The HO06 section (14°34'45.2" N 105°16'30.0" E) is located near the southeastern margin of the Khorat Plateau Basin about 15 km southwest of Huai Om, where Fiske et al. (1996) reported MN tektite fragments at the top of the "laterite" layer (Fig. 2.2A). The section is exposed along the spillway of Huai Phueng and Phlan Suea Ton Lang reservoirs (Fig. 2.2B). The weathered Cretaceous sedimentary basement and overlying Quaternary

deposits are exposed laterally for at least 200 m along both banks of the spillway. A cluster of MN tektite fragments was found in the section at the north bank (Fig. 2.2B). Any evidence of tectonic disturbance of the Quaternary deposits and the basement was not found.

2.3 Methods

2.3.1 Field survey and sampling

A field survey was conducted at the HO06 section to describe the occurrence of the cluster of MN tektite fragments found in the "laterite" layer. The observation of the lithostratigraphy of the Quaternary deposits was conducted at the southern bank of the spillway, where the sequence from the basement sandstone to the top of the Quaternary deposit is exposed (Figs.2.2B, 2.3). The detailed lithostratigraphy of the Quaternary deposit in this region is provided for the Huai Om section described in section **3.4.1** in this thesis.

A block sample of 25 x 15 cm area with 10 cm thickness was taken from the area where the cluster of MN tektite fragments was found using a handheld electric cutter for three-dimensional CT scanning. After taking the block sample in the field, I further recovered MN tektite fragments by gradually expanding the excavation area until no large (> 1 cm diameter) tektite fragments were found. A ca. 40 x 30 cm area was excavated in the end. There is a possibility that small (< 1 cm diameter) tektite fragments spread further away were overlooked. After the CT scanning, the block sample was dismantled in the laboratory, and MN tektite fragments larger than 5 mm in diameter were recovered in the laboratory.

2.3.2 Measurement of major element compositions of the MN tektite fragments

The major element compositions of nine selected MN tektite fragments found at HO06 section were analyzed by EPMA on thin sections using a JEOL JXA-8900L electron probe microanalyzer at the Department of Earth and Planetary Science, the University of Tokyo. The analysis was performed using 7.5 nA beam current and 15 kV accelerating voltage with a defocused electron beam of 5 μm. Counting times were 5 s on the background and 10 s on peak. Si, Al, Fe, Mg, K, Ca, Na, Ti, and Mn were analyzed.

To reduce possible volatilization effects, potassium and sodium were analyzed before other elements, followed by the method of Glass et al. (2020). The error of the analysis was evaluated by analyzing the composition-known magnetite that was repeated ten times. The analytical error was better than 0.5 % in concentration for all elements.

In each thin section, 10 to 20 points were measured. Since the total percentage of measured elements varies between 96 and 100 wt.%, I selected data, the total percentage of which is larger than 98 %, to calculate an average and standard deviation of the major element composition of each thin section. After the data screening, each thin section still has 10 to 15 measured points. The standard deviation of the major element compositions, which is 1.3% in maximum (Table 2.2), includes the heterogeneity of the sample and the measurement error.

2.3.3 Size distribution analysis of the MN tektite fragments

The size distribution of fragments is often used to investigate the fragmentation processes (e.g., Farris and Paterson 2007; Bjørk et al. 2009; Roy et al. 2012). Fracturing or crushing of rock or glass results in size distributions of fragments that can be represented by power-law functions in which fragment frequency increases with a decrease in fragment size, because of scale invariance of the fragmentation process (e.g., Turcotte 1986). The relationship between cumulative frequency and fragment size can be described by the power-law equation

$$N_{(\geq r)} = kr^{-Ds} \tag{2.1}$$

where r is a radius of a fragment, $N_{(\geq r)}$ is the number of fragments with a radius greater than r, and k is a fitting parameter. The power exponent Ds is the fractal dimension for the fragment size distribution.

The size and weight of the MN tektite fragments were recorded in the laboratory. The long, intermediate, and short axes (a, b, and c axes) defined as the dimensions of a fragment in three mutually orthogonal planes (a > b > c) were measured using a caliper with an accuracy of 0.05 mm.

2.3.4 CT scanning of the brock sample

X-ray CT scanning of the block sample was conducted using micro-CT scanner TESCO TXS320-ACTIS at the National Museum of Nature and Science, Tokyo, with an X-ray beam at 290 kV and 200 μA. The block sample was scanned at a slice thickness of 0.3 mm, yielding 1912 slices. Voxel (3D-pixel) sizes are 0.1758 x 0.1758 x 0.3 mm. The obtained data in DICOM format were imported into Amira 5.4.3 software for 3D imaging. MN tektite fragments were separated using the segmentation editor in Amira 5.4.3 based on the contrast in X-ray transmittance between tektite fragments and the surrounding matrix. Tektite fragments larger than 1 cm were identified because smaller tektite fragments are more difficult to recognize on the CT cross-sections. The identification of the tektite fragments on the CT cross-sections was confirmed by comparing each tektite fragment to the tektite fragments recovered from the dismantled block sample.

Before conducting the CT scanning of the block sample, one MN tektite fragment (HO06MN33) without any matrix material adhered, and fragments adhered with cemented surrounding matrix (HO06MN163) were also subjected to X-ray CT imaging with a slice thickness of 0.2 mm, to see how MN tektite fragments appear in CT scan cross-sections (Fig. A1.1).

2.4 Results

2.4.1 Lithostratigraphy

The basement rock at the HO06 section is weathered very fine quartzo-feldspathic sandstone of the Cretaceous Khok Kruat Formation in the uppermost part of the Khorat Group (Nuchanong et al. 2014). The thickness of the exposed part of the basement sandstone is approximately 2 m and is exposed continuously along the spillway. The basement sandstone dips approximately 10° to the west (Fig. 2.3).

The Quaternary deposits unconformably overlying the Cretaceous basement sandstone can be divided into three lithostratigraphic units (Units 1 to 3 in ascending order) (Fig. 2.3). Unit 1 is a whitish-gray silty very fine sand layer of 70 cm thickness. The basal contact with the basement is sharp, largely horizontal, slightly undulating, and forms an angular unconformity (Fig. 2.3). Unit 2 is a reddish-brown, poorly-sorted, granule- to pebble-bearing medium to coarse sand layer of 55 cm thickness. It overlies Unit 1 with a sharp and generally planar contact with no evidence of erosion. The gravel

clasts are 0.2–3 cm in diameter and composed mainly of white quartzite pebbles and their fragments (Fig. 2.4B). This unit is partly cemented by reddish-brown iron oxides to form reddish-black pebble size spherical to irregular shaped nodules, which is consistent with the descriptions of the "laterite" layer (e.g., Songtham et al. 2011, 2012). Unit 3 is a whitish- to brownish-gray massive fine sand layer. The thickness of this unit is 2 m (Fig. 2.4A). The basal contact is sharp and planar, with no evidence of erosion. This unit is capped by ca. 20 cm thick modern soil with a gradational contact. The cluster of the MN tektite fragments was found in the upper part of Unit 2 (ca. 10 cm below the upper boundary) (Fig. 2.5).

2.4.2 Description of the MN tektite fragments

The MN tektite fragments found at the HO06 section are black-colored vesicular glass fragments showing submillimeter-scale layering (Fig. 2.6). Under an optical microscope, thin sections of the fragments show layering composed of the dark brownish-colored and light greenish-colored glass stripes parallel to each other. Each stripe has micrometer-scale subparallel lamination characterized by an alternation of dark-brownish and pale-greenish lenses. Elongated vesicles of submillimeter size are occasionally observed, the long axes of which are roughly parallel to the layering (Fig. 2.7). Mineral inclusions, which are several micrometers in diameter, are sparsely contained, but they are too small to identify mineral species under an optical microscope. These characteristics are consistent with the descriptions of Australasian MN tektites reported in the Indochina Peninsula (e.g., Wasson 1991; Glass et al. 2020).

In total, 331 MN tektite fragments were found in the small area (~40 cm x 30 cm with 10 cm in thickness) in the upper part of Unit 2 (One-hundred and seventy-seven fragments were collected in the field after taking the block sample, and 154 fragments were collected from the dismantled block sample in the laboratory). The total weight of the fragments is at least 713 g (Table A1.1).

The a, b, and c axes of the MN tektite fragments range from 2.00 to 52.80 mm, 1.95 to 40.00 mm, and 0.70 to 30.80 mm, respectively. The average lengths and standard deviations (in parenthesis) are 16.3 (8.7), 11.3 (7.1), and 7.2 (5.5) mm, respectively. These large standard deviations of the size of the MN tektite fragments correspond to "very poor sorting" in the scale of sorting for sediments (Folk and Ward 1957). The fragments are

very angular, and fragile edges are well preserved, as shown in Figure 2.6. Forty-six large fragments recovered from the dismantled block sample and seven large fragments recovered in the field (53 tektite fragments in total) are fitted together like a jigsaw puzzle to form a large MN tektite mass. The restored MN tektite mass is an ellipsoidal shape of ~370 g in weight (Fig. 2.8). The rest of the fragments are too small and so many that it is difficult to find their positions to restore the original tektite mass. However, the restoration result strongly suggests that tektite fragments forming the cluster originally composed one large tektite mass of >713 g weight. The majority of the outermost surface of the restored tektite mass was peeled off, showing the section of the internal layered structure (Fig. 2.8B), while a typical pitted and grooved surface similar to those in splash-form tektites was observed in some part (Fig. 2.8C) suggesting that the original surface of the tektite mass is partly preserved. The fracture surfaces of the MN tektite fragments are matt compared to a fresh fracture surface because of the presence of small pits, as shown in Figure 2.8D. These matt surfaces of tektites were formed by soil etching after their burial (Rost 1969; La Marche et al. 1984), indicating that the fragmentation occurred in the geological past. Most fragments have iron-oxide cement and calcite cement, in some cases adhering to the fragment surfaces. Some vesicles open to the surface are filled with the iron-oxide and calcite cement materials, indicating that the laterization of Unit 2 occurred after their fragmentation.

2.4.3 Major element composition of the MN tektite fragments

The major element compositions of nine MN tektite fragments from the HO06 section, with their average compositions and standard deviations, are shown in Table 2.2. The major element compositions of these samples are within the range of compositions of previously reported MN tektites from Ubon Ratchathani province within 1σ, for most elements (Glass and Koeberl 1989; Koeberl 1992; Fiske et al. 1996; Herzog et al. 2008) (Fig. 2.9), indicating that the fragments found at HO06 section are surely Australasian MN tektites.

Figure 2.9B is diagrams showing SiO_2 vs. Al_2O_3, FeO, K_2O, and MgO concentrations of the nine MN tektite fragments from the HO06 section compared with concentrations of previously reported Australasian MN tektites from Ubon Ratchatani province (Glass and Koeberl 1989; Koeberl 1992; Fiske et al. 1996; Herzog et al. 2008).

The major element compositions of the nine fragments are closely plotted in a narrow area and indistinguishable from each other within 1σ, indicating that these tektite fragments have similar chemical compositions.

2.4.4 Size distribution of the MN tektite fragments

Figure 2.10 shows the cumulative size distribution of the MN tektite fragments larger than 10 mm found from the HO06 section. The size of the fragments is represented by the equivalent spherical diameter ($r = \sqrt[3]{abc}$). The cumulative size distribution increases rapidly from 37 to 26 mm and then increases slowly in a range smaller than 26 mm, showing a bi-fractal distribution that follows two different power laws. *Ds* for the range from 10 to 26 mm is 2.2, and *Ds* for the range from 26 to 37 mm is 7.5. The position dividing the two power laws is determined by adjusting the dividing point every 0.5 cm to maximize the average of the R^2 values. The bi-fractal size distribution implies that the fragment size distribution was affected by two different fragmentation mechanisms (e.g., Schultz and Gault 1990).

It is known that *Ds* for the fragments generated by fragmentation of rocks or glass is roughly proportional to the intensity of the fragmentation process. Although *Ds* is also affected by the inherent strength properties of the rock or glass, fragments generated by a higher magnitude and rate of stress loading tend to have higher *Ds* value (e.g., Takagi et al. 1984; Jébrak 1997; Roy et al. 2012; Xu 2018). For instance, *Ds* for rock fragments generated by weathering of andesite in the field or hammering of limestone by hand is 2.5-2.7 (calculated from the data of Domokos et al. 2015). *Ds* for rock fragments generated by rockfalls and rock avalanches with various lithologies is 1.6 to 4.7 (Crosta et al. 2007; Ruiz-Carulla and Corominas, 2020). The size distribution of rock fragments generated by complete fragmentation of target rocks in hypervelocity impact experiments shows bi- or tri- fractal distributions, in which *Ds* for the finer fraction ranges from 1.7 to 4.3 and *Ds* for the coarser fraction ranges from 4.8 to 11.9 (calculated from the data of Takagi et al. 1984; Michikami et al. 2016). *Ds* for the fragments of a block on the lunar surface fragmented by a small meteorite impact is 3.3 to 6.0 (Ruesch et al. 2020).

Although the difference of physical properties between the tektite glass and rocks needs to be considered, the high *Ds* (7.5) for the coarse fraction of the tektite

fragments is higher than the range of *Ds* previously reported for rock fragments generated by rockfalls and rock avalanches and similar to *Ds* of the coarser fraction fragments generated by hyperspeed impact experiments and impact fragmentation on the lunar surface. This high Ds value indicates that the tektite fragments were formed through intense fragmentation by a relatively high energetic process.

2.4.5. Observation of the CT scan 3D image of the block sample

In CT cross-section images, tektite fragments appear as angular-shaped areas with moderate X-ray transmittance, exhibiting elongated vesicles (Fig. A1.1). The CT scan 3D image of the block sample revealed that the MN tektite fragments are distributed in 20 x 10 x 10 cm space as if they were expanded from the original tektite mass by fragmentation (Fig. 2.12). The large fragments are not closely contacted but separated from each other by 1 to 2 cm (Fig. 2.12), implying that these fragments were not fractured by a thermal break-up after burial. If these large fragments were fractured by a thermal break-up after burial, the fragments should be closely contacted.

Figure. 2.12 shows the comparison of fragments in CT scan 3D image and in the restored MN tektite mass. The tektite fragments fitted together in the restored tektite mass are closely positioned in the CT scan 3D image. There are several pairs of the fragments facing their fracture surfaces (Fig. 2.12). These characteristics strongly suggest that the MN tektite fragments were not disturbed at all after the fragmentation.

2.5 Discussion

2.5.1. Fragmentation process of the MN tektite fragments

The fact that the large tektite fragments fitted together to form one large ellipsoidal tektite mass with the original surface partly preserved, as well as the similar chemical composition of the MN tektite fragments, indicates that the tektite fragments were formed by fragmentation of one large tektite mass. The very angular shapes with well-preserved fragile edges, the very poorly sorted nature of the MN tektite fragments, and the occurrence that the tektite fragments forming a cluster suggest that these MN tektite fragments were not transported a long distance but rather fragmented in situ. The presence of the pairs of the fragments facing their fracture surfaces (Fig. 2.12) suggests that the MN tektite fragments were not disturbed after the fragmentation and burial.

Fiske et al. (1996) interpreted that the fragmentation of an original MN tektite mass was a low-energy process such as weather or climate-related temperature-induced fracturing after the deposition of the MN tektite mass based on the close spatial association of the MN tektite fragments at Huai Sai. However, as is mentioned in the previous section, the size distribution of the coarse fraction of the MN tektite fragments from the HO06 section suggests a relatively high energy process rather than a low energy process. The possibility that the MN tektite mass was broken by tectonic movement after deposition is also unlikely because any evidence of tectonic deformation was not found at the outcrop. The other possibility is that the fragmentation occurred by a high-speed collision of ejecta materials during the flight before the deposition. However, this possibility is also unlikely because if the fragmentation occurred during the flight, the fragments would have separated before they landed on the ground and would not have formed a cluster. Consequently, the timing of the fragmentation of the MN tektite mass is constrained to the time of the landing on the ground.

To be fragmented at the landing on the ground, the tektite mass needs to be quenched under the glass transition temperature before the landing. Assuming that the tektite is ballistically ejected at 45° from the impact site and that the distance from the impact site is 100 km, the time of flight can be estimated as ~144 s (Collins et al. 2005). This should be the minimum estimate considering the presence of atmosphere in the actual case. The quench time of the tektite can be roughly estimated by assuming that the tektite is a spherical black body with a 9.4 cm diameter (~1 kg) (Greenland and Lovering 1962). The estimated time to quench the tektite from 1900 K (Walter 1965; Cavosie and Koeberl 2019) to the glass transition temperature of MN tektites (1005 K; Klein et al. 1980) is ~164 s. Thus, the estimated time of flight and the estimated time of quench to the glass transition temperature is roughly comparable. Since the surface area of the MN tektite mass must be much greater than that of a simple sphere, the MN tektite mass is considered to be quenched more efficiently. Thus, the temperature of the MN tektite mass is considered to be significantly lower than the glass transition temperature at the time of the landing. Thus, the proposed process that requires the tektite mass had quenched at the time of the landing is consistent with the time of flight.

The MN tektite fragments were considered to have been either co-deposited with other ejecta materials immediately after (or almost at the same time with) the fragmentation or the MN tektite mass was fragmented during penetration into the

unconsolidated ejecta of Unit 2 so that the fragments remained as a cluster.

As for the fragmentation mechanism of the finer fraction of the MN tektite fragments, one possibility is that some of the tektite fragments were further fractured by weather or climate-related thermal fracturing after the deposition. Another possibility is that some of the tektite fragments generated by the collision with the ground surface were secondarily fractured by collision with the surrounding other ejecta materials immediately after the first fragmentation.

The other possibility for the fragmentation mechanism of the finer fraction is raised from the relationship between the size and shape of the fragments. In hypervelocity impact experiments, the fragments generated by complete fragmentation of the target rock show bi- or tri-fractal size distribution, in which fine and coarse fractions follow different power laws (Takagi et al. 1984; Onose et al., 2011; Michikami et al. 2016). It is also known that the average ratio of the three axes a: b: c of the fragments generated by hyper-velocity impact experiments generally are ~2: $\sqrt{2}$:1 (corresponding to c/a=~ 0.5, b/a=~0.7) (e.g., Capaccioni et al. 1986; Capaccioni et al. 1984; Fujiwara et al. 1978; Michikami et al. 2016). Onose et al. (2011) conducted hyper-velocity impact experiments on the gypsum target and reported that larger fragments tend to have equant shapes with similar a, b, and c axis, while smaller fragments tend to have flat or bar-like shapes. Based on this relationship between the shape and size of the fragments, Onose et al. (2011) interpreted that the larger fragments were generated by radial cracking of the target, and the smaller fragments were generated by spallation from the target surface resulted in different power-law size distributions and different shape characteristics for large and small fractions of the fragments. Fig. 2.11 is a diagram showing b/a versus c/a of the MN tektite fragments at the HO06 section. Although the ratio of the three dimensions of the fragments is various, the average ratio of the three axes is c/a=0.43, b/a=0.69, which is similar to that of the fragments generated by hyper-velocity impact experiments. It is also clear that the shapes of the fragments smaller than 26 mm tend to be flat or bar, while large fragments (> 26 mm in sphere equivalent diameter) are mostly equant shapes. This size-shape relationship of the MN tektite fragments at the HO06 section and the fact that the most surface of the restored tektite mass was peeled off, showing the sections of the internal layered structure (Fig. 2.8), imply the possibility that small fragments were generated by peeling off from the surface of the original MN tektite at the collision with the ground. However, it is unlikely that the MN tektite mass was fragmented by a hyper-

velocity (more than several hundred meters per second) impact to the ground because the fragments would have been scattered and not buried as a cluster if they impacted at such a high speed. In any case, I can conclude that the whole size distribution of the MN tektite fragments, especially the high *Ds* value of the coarse fraction, is different from the size distributions of rock fragments generated by low energy processes.

2.5.2. Stratigraphic position of Australasian tektites in Indochina Peninsula

As proposed in the previous sections, the fragmentation of the MN tektite mass occurred at the time of the landing on the ground. The fragments were buried immediately after the fragmentation by co-deposition of other ejecta materials or penetration into the ground covered by unconsolidated ejecta deposit. In either case, the fragments were preserved as a cluster. Thus, the MN tektite fragments in the upper part of Unit 2 ("laterite" layer) at the HO06 section are considered in the primary position (i.e., in situ).

Fiske et al. (1996) interpreted that MN tektite fragments found at the top of Unit 2 at the Huai Om and Huai Sai sections were reworked because, in their opinion, the upper surface of Unit 2 is a paleo-erosional surface. However, it is not consistent with this interpretation that MN tektite fragments are found not at the top of Unit 2 but within Unit 2 at the HO06 section. The distribution of the tektite fragments in sediments as if they were expanded from the original tektite mass by fragmentation (Fig. 2.12) is also not consistent with the previous interpretation because if reworked on the paleo surface, the fragments would be distributed on a plane. In addition, there was no evidence of erosion at the top of Unit 2 at the HO06 section and several other sections in the region (detail in section **4.3** of this thesis). Furthermore, our field observations of the "laterite" layer in other sites (for example, an active sandpit at Noen Sa-nga in Chaiyaphum province) suggest that laterization (precipitation of iron hydroxides) of this layer could have occurred within a few years after road cuts or pit walls were formed, indicating that the hard-cemented appearance of this layer was not formed as an erosional pavement before the impact, but formed on the outcrop surface by recent ferricretization (detail in **4.3.1.1**). Koeberl and Glass (2000) and Keates (2000) pointed out that the Australasian tektites in Australia are generally found in deposits younger than the age of the impact, and interpreted by analogy that the tektites reported in the "laterite" layer in Indochina may be of similar reworked origin. However, this analogy is not based on observational

evidence in Southeast Asia. The in-situ occurrence of the MN tektite fragments in Unit 2 at the HO06 section and the fact that the MN and splash-form tektites generally were reported in the upper part of or at the top of the "laterite" layer at sites in the broad area of eastern Indochina (Table 2.1, Fig. 2.1) strongly suggest that the Australasian tektites found from the "laterite" layer were deposited in situ as ejecta and the "laterite" layer is a part of the proximal ejecta deposit of AATE.

2.6 Summary

I described the detailed occurrence of the cluster of MN tektite fragments found in the upper part of the "laterite" layer at the HO06 section, Ubon Ratchathani province, northeastern Thailand. At least 331MN tektite fragments (total weight of >713 g) were concentrated in a small (40 x 30 cm) area with 10 cm in thickness. The occurrence as a cluster, the very angular shapes, the very poorly sorted nature of the fragments, the restoration of the part of the original MN tektite mass, and the similar chemical composition of the fragments suggest that these MN tektite fragments were not transported long distances but rather fragmented in situ.

The size distribution of the MN tektite fragments shows bi-fractal, following two different power laws in the range 10 to 26 mm and 26 to 37 mm with *Ds* of 2.2 and 7.5, respectively. The high *Ds* for the coarse fraction of the tektite fragments implies that the tektite fragments were formed through intense fragmentation by a relatively high energy process. The CT scan analysis of the block sample revealed that the MN tektite fragments were buried immediately after the fragmentation and not disturbed after the burial.

These results suggest that the tektite fragments were formed by fragmentation of one large tektite mass at the time of the landing after the ejection by the impact and has not been disturbed further (i.e., in situ). This conclusion is contrary to the previous interpretation that similar tektite fragments were reworked on the upper surface of the "laterite" layer, which was interpreted as a paleo-erosional surface (e.g., Fiske et al. 1996), but strongly suggests that the "laterite" layer distributed widely in the eastern Indochina is a part of the proximal ejecta deposit of the AATE.

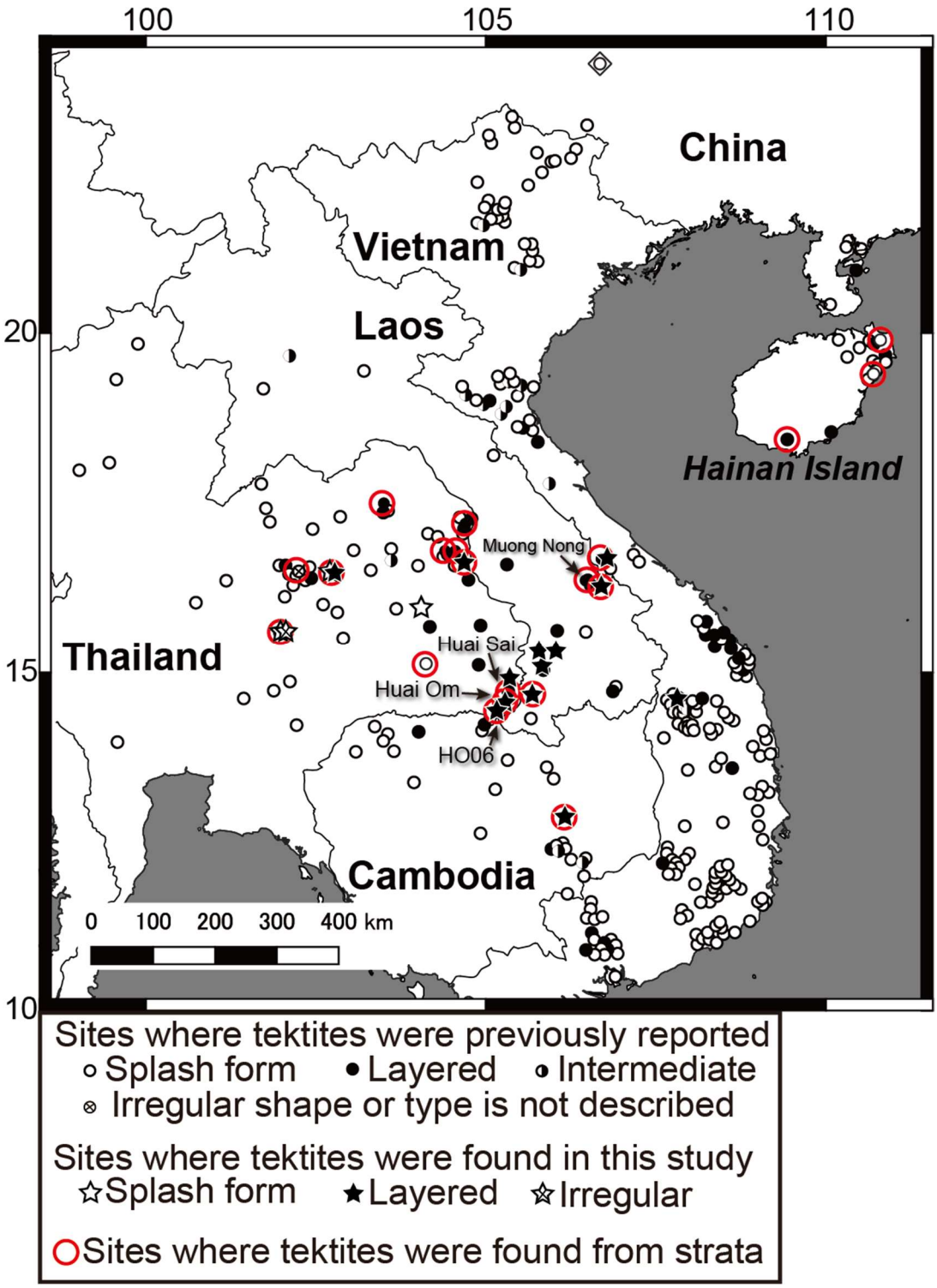

Figure 2.1 Map of Indochina showing sites where Australasian tektites have been found. Sites where the tektites were found from strata, are also shown (after Schnetzler 1992 and references listed in Table 2.1). The names of locations mentioned in Chapter 2 are also shown.

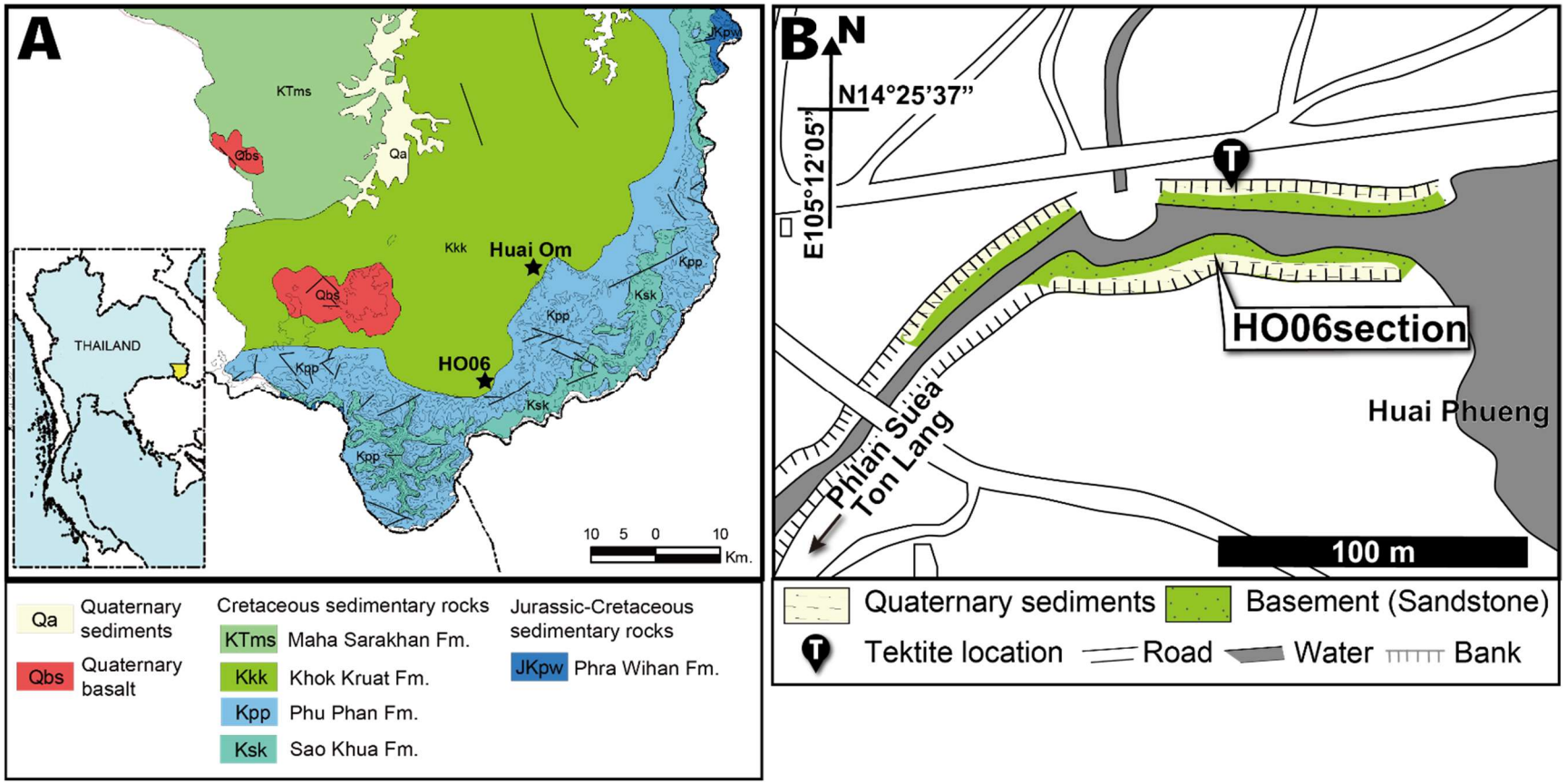

Figure 2.2 Geological map of the southern part of Ubon Ratchathani province, northeastern Thailand (A) (after the geological map of Thailand by province made by Department of Mineral Resources of Thailand (http://www.dmr.go.th/n_more_news.ph p?nid=79591, accessed 15/12/2020)) and locality map of the HO06 section (B). The location where the cluster of MN tektite fragments was found is also shown.

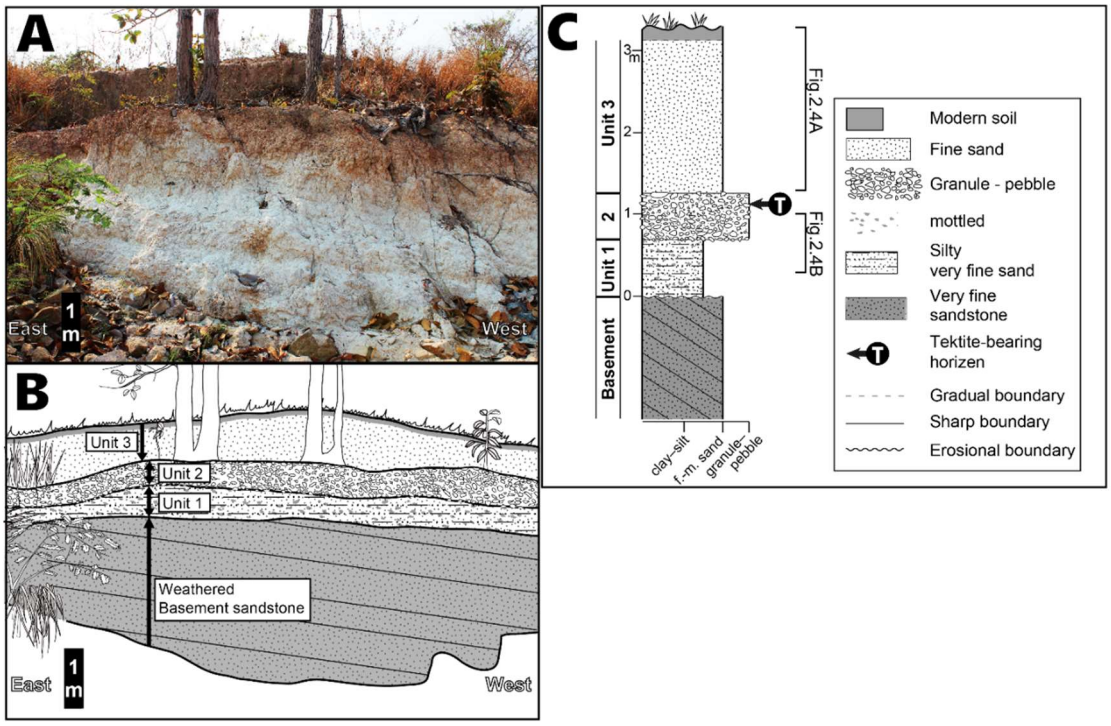

Figure 2.3 Field photographs and the columnar section of the HO06 section. A) Field photograph of the section on the southern side of the spillway. B) Cartoon of the stratigraphy shown in B. The legend B is the same as that for C. C) Columnar representation of the stratigraphy section made on the southern side where a good exposure was observed. Note the stratigraphic position of the MN tektite fragment cluster, which was found in the upper part of Unit 2 on the northern side of the spillway.

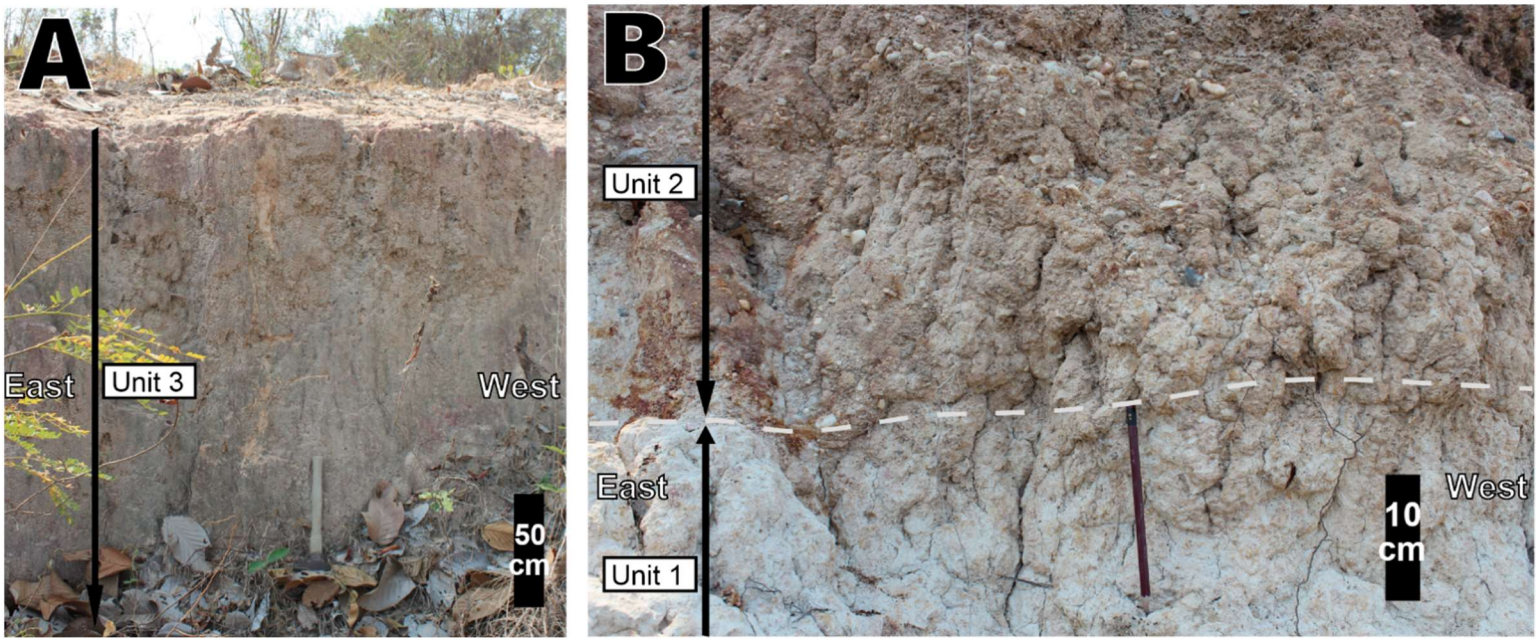

Figure 2.4 Field photographs of the HO06 section. A) Close photograph of Unit 3. B) Close photograph of Unit 1 and Unit 2.

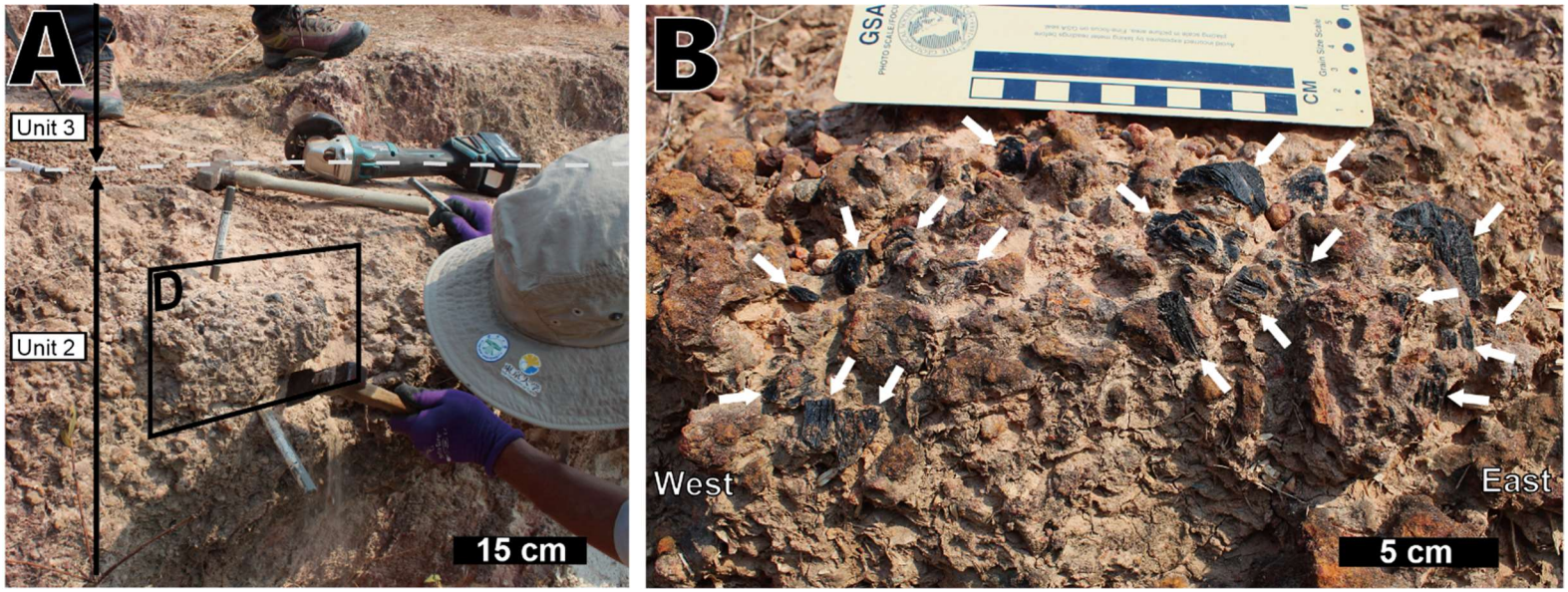

Figure 2.5 Field photograph of the cluster of tektite fragments within the upper part of Unit 2. A) A wider photograph showing that the cluster of tektite fragments are ca. 10 cm below the upper unit boundary. B) The white allows point to each fragment partly exposed on the outcrop surface.

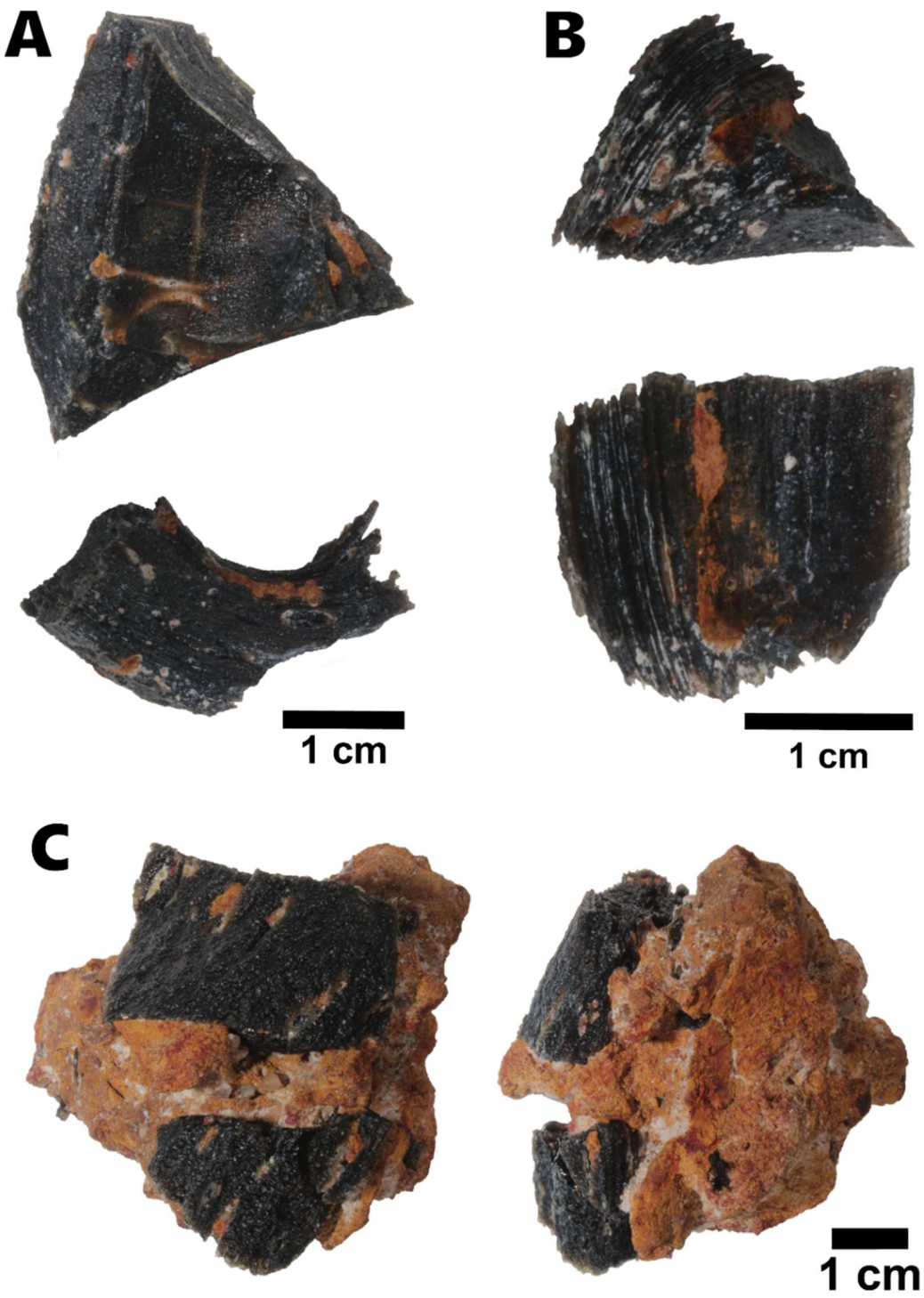

Figure 2.6 Photographs taken of differing orientations of examples of the tektite fragments recovered from the HO06 section. A) Sample HO06MN34. B) Sample HO06MN79. C) Sample HO06MN32_a and 32_b. The MN tektite fragments are black vesicular glass showing layering structure and have angular shapes with fragile edges.

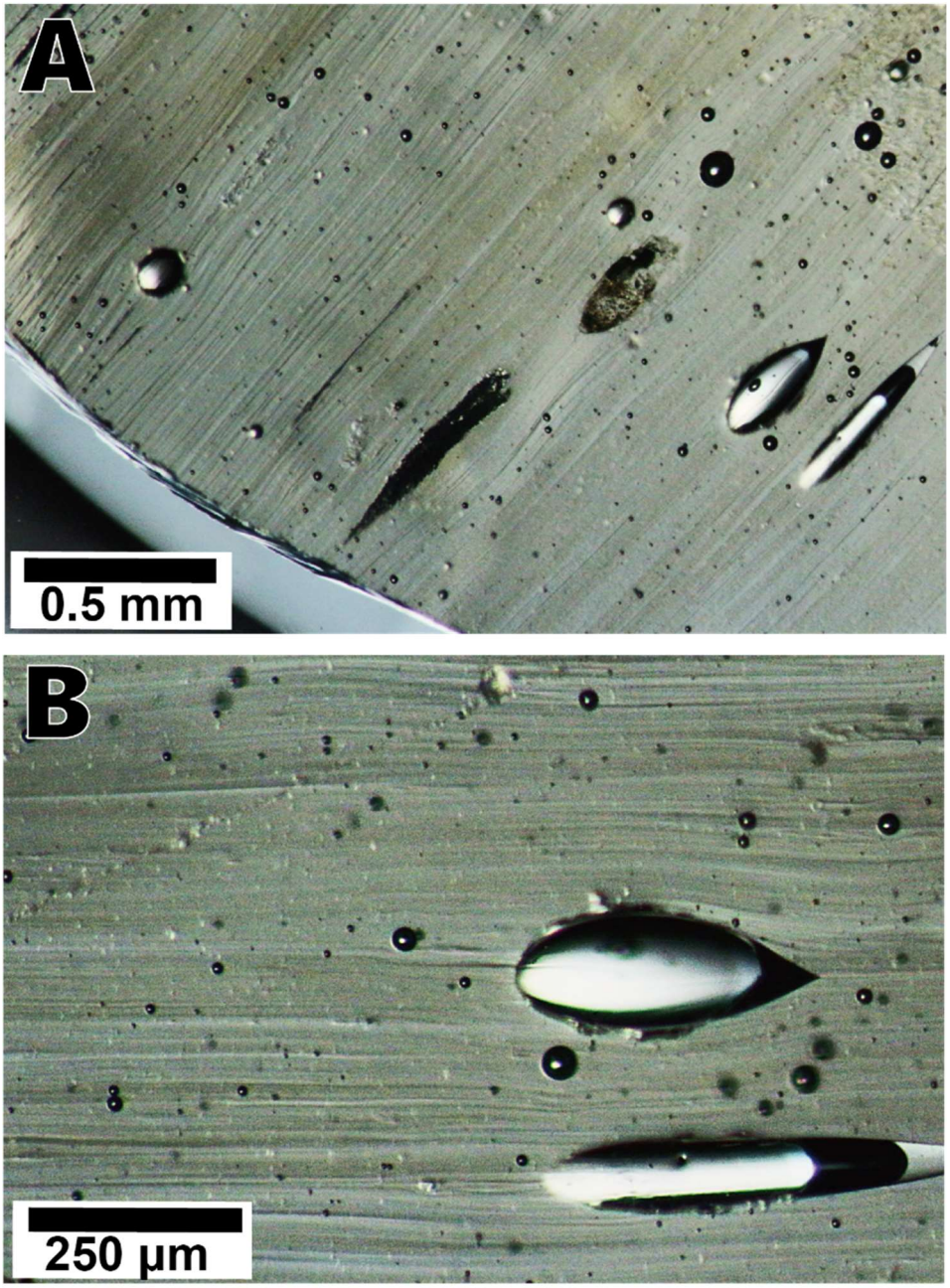

Figure 2.7 Thin section photographs of sample HO06MN12 (the contrast of the photographs is enhanced). The layering texture is composed of the dark- and light-colored glass lenses, and the elongated vesicles are shown. A) Lower magnification view showing submillimeter-scale alteration of dark and light stripes. B) Higher magnification view of the same section in A.

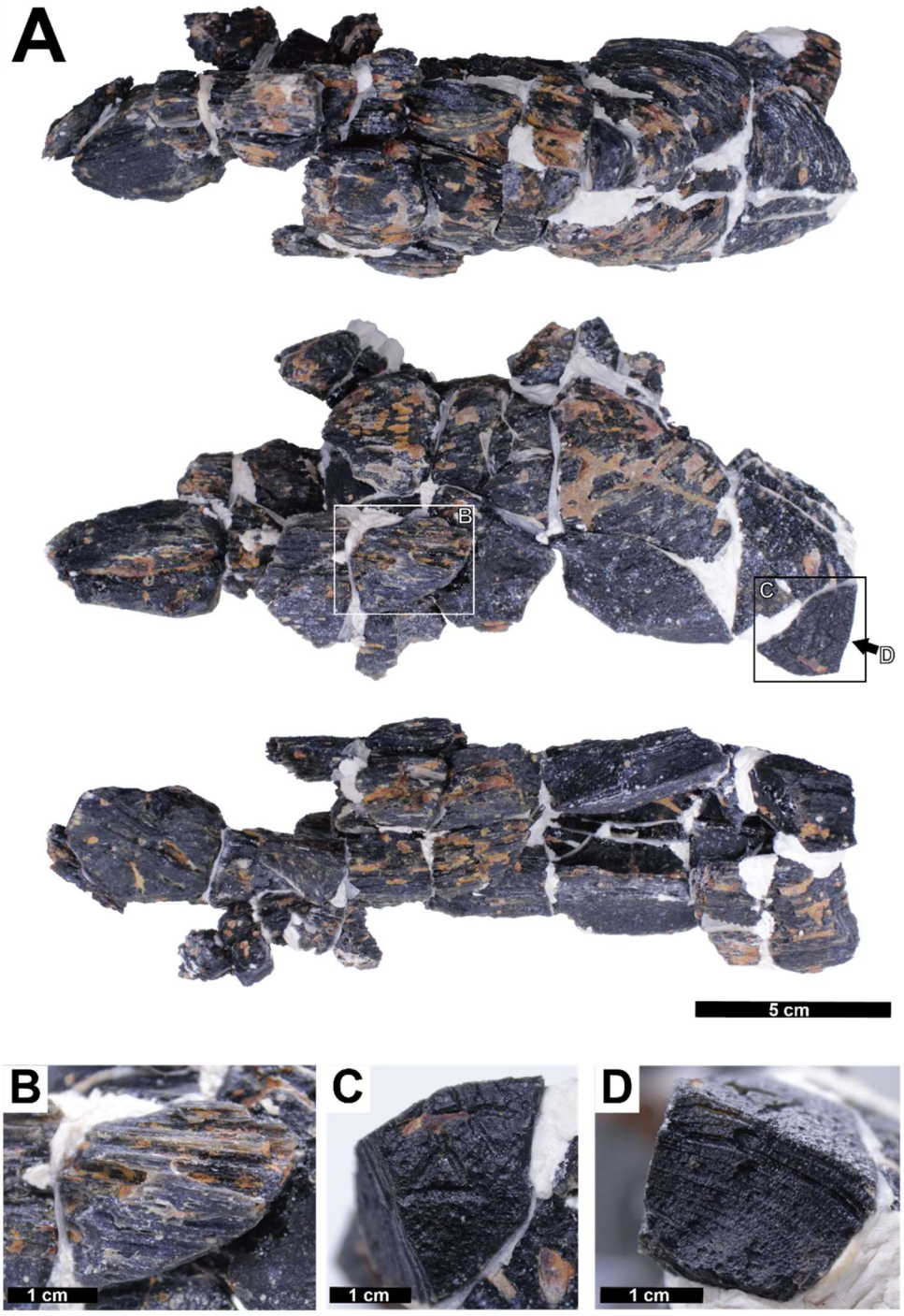

Figure 2.8 The photographs taken of different orientations of the restored tektite mass(A). B) Photograph of a part of the surface, which was peeled off showing the section of the internal layered structure cut by low angle. C) Photograph of a part of the surface, which is considered as the preserved original surface of the tektite mass showing a typical pitted and grooved surface. D) Photograph of the fracture surface of the MN tektite fragment, which is matt due to the presence of small pits.

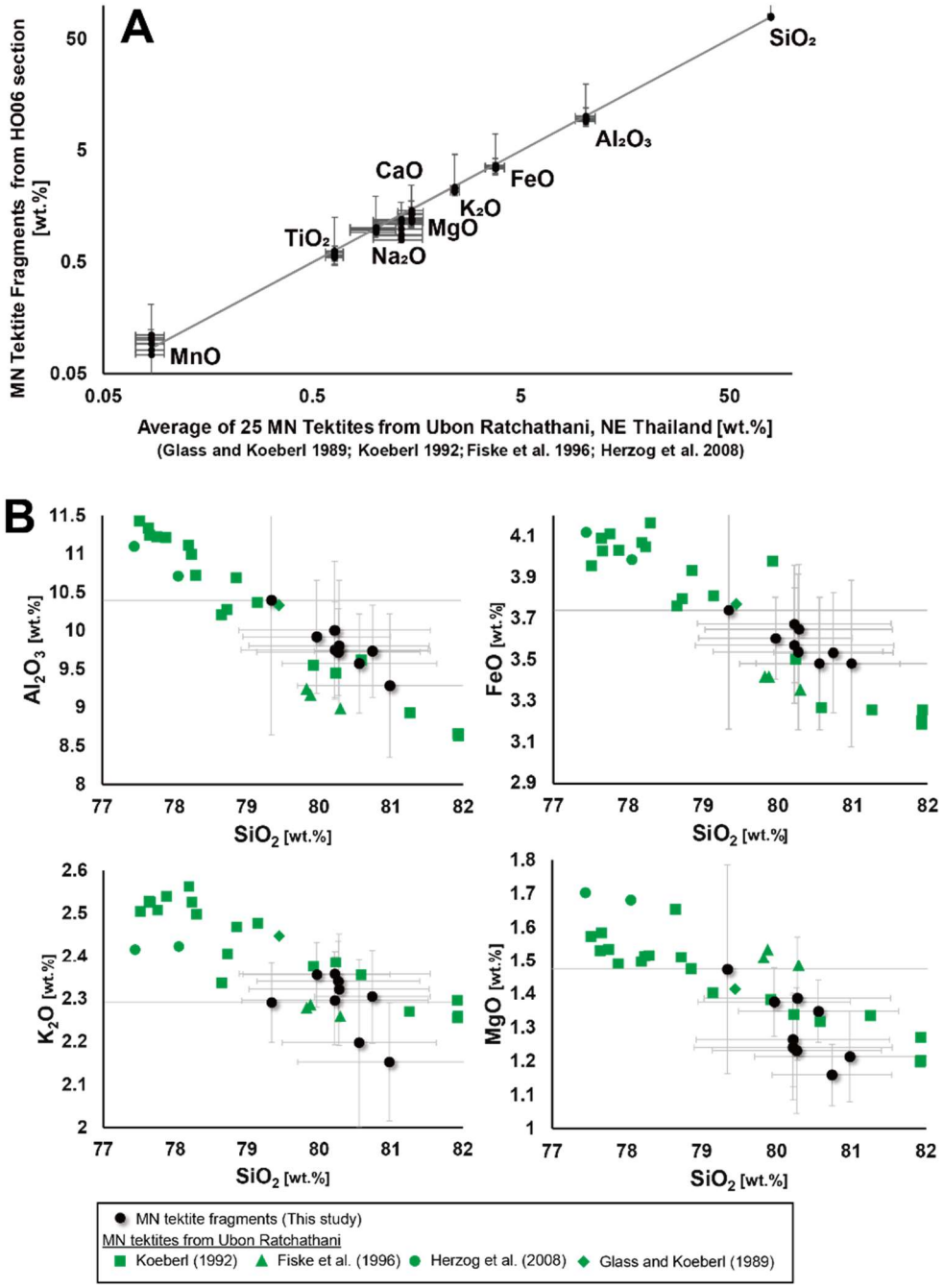

Figure 2.9 Major element compositions of the MN tektite fragments from the HO06 section. A) Comparison of the major element compositions of the MN tektite fragments from the HO06 section and the average of other MN tektites from the same region, Ubon Ratchathani province, previously reported. B) X–Y plots of the concentrations of SiO_2 versus Al_2O_3, FeO, K_2O, and MgO of the MN tektite fragments from the HO06 section compared with other MN tektites from the same region, Ubon Ratchathani province, previously reported. The error bars represent 1σ of ten to fifteen measurements of each section.

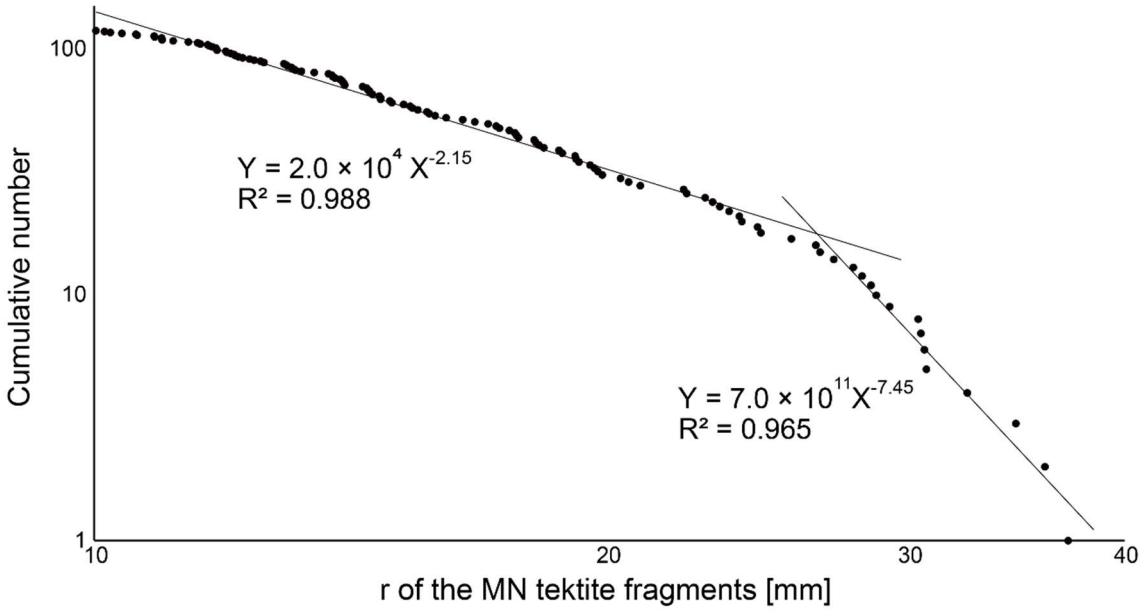

Figure 2.10 Cumulative size distribution of the MN tektite fragments from the HO06 section for the size range of r > 10mm.

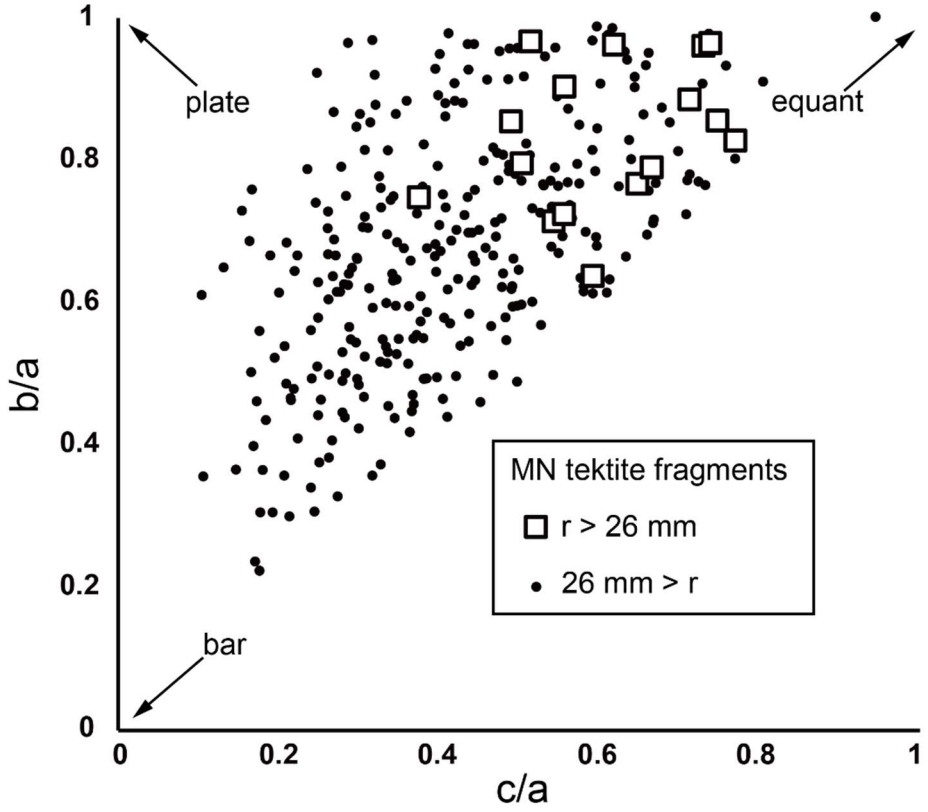

Figure 2.11 Shape distribution of the MN tektite fragments from the HO06 section.

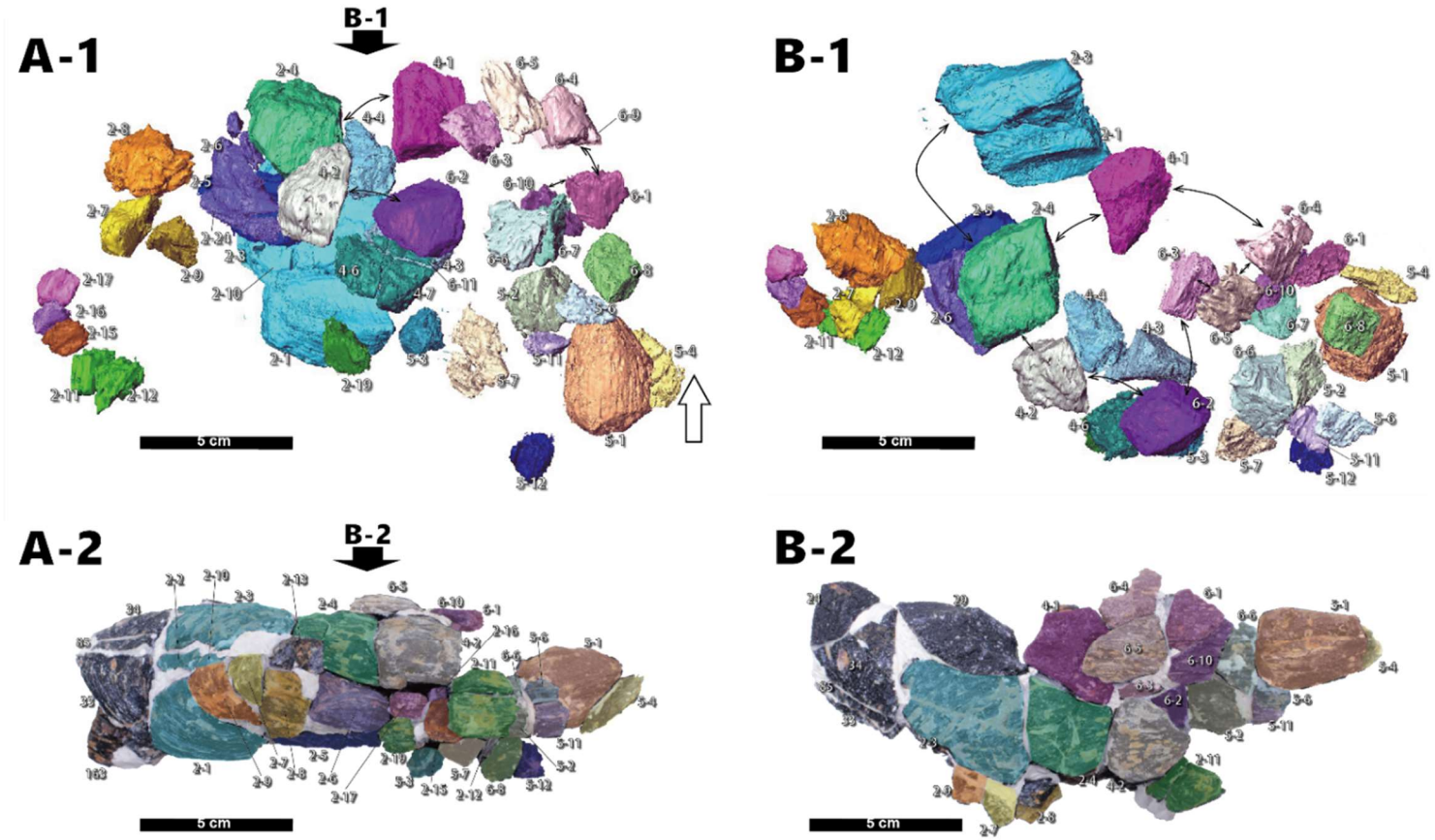

Figure 2.12 Comparison between CT scan 3D image of the MN tektite fragments in the block sample (A-1 and B-1) and the restored tektite mass (A-2 and B-2) from different orientations. The fragments in the restored mass which appear in the CT scan 3D image are represented by the same color in the CT scan 3D image. Several pairs of fragments were buried as facing their fracture surfaces, indicated by double-headed arrows. The white arrow on the CT scan 3D image represents the stratigraphic upper direction.

Table 2.1 Sites in Indochina where Australasian tektites were reported in strata

Locality	Country	Latitude	Longitude	Tektite type	Ocurrence	Reference
Phang Daeng*	Thailand	N16°48'	E104°24'	MN	At least 10 kg of MN tekitte fragments were found in the "laterite" layer, ~0.3 m below the surface. Tektite fragments were concentrated in a small area.	Barnes and Pitakpaivan 1962
Nong Sapong *	Thailand	N17°12'	E104°42'	MN	MN tektite fragments were found in the "laterite" layer, ~0.7 m below the surface. Tektite fragments were concentrated in a small area.	Barnes and Pitakpaivan 1962
81 km west of Nakhon Sakhon*	Thailand	N17°30'	E103°30'	MN	MN tektite fragments were found in the "laterite" layer, ~0.7 m below the surface.	Barnes and Pitakpaivan 1962
Huai Sai	Thailand	N14°53'	E105°25'	MN	A cluster of 1139 MN tektite fragments with a total mass of 6 kg were partly exposed at the surface. The largest piece weighed 701.7 g. The fragments were concentrated in 2 x 3 m area and 30 cm in depth. These fragments were in the uppermost light gray sandy soil layer and in the upper 10 cm of the quartz pebble-bearing "laterite" layer. Most of fragments were found at the boundary of these two layeres.	Fiske et al. 1996
Huai Om	Thailand	N14°35'	E105°17'	MN	Two MN tektite fragments with total weight of 2 g were found from the top of the "laterite" layer. 14 MN tektite fragments with total weight of 43.5 g were in float but clealy derived from the immediate strata above.	Fiske et al. 1996
1 km WNW of Ban E Sae	Thailand	N15°07.0'	E104°07.0'	Sp	Two splash form tektites were from the very top of the "laterite" layer.	Wasson et al. 1995
400 m NNW of Ban Ta Ko	Laos	N16°22.336'	E106°27.595'	MN	MN tektite fragments were found in the upper 20 cm of the pebbly "laterite" layer, ~1 m below the surface. 450g of tektite fragments were found in total from 12 square meters area.	Fiske et al. 1999
500 m N of the entrance of Muong Nong	Laos	N16°22.800'	E106°30.00'	MN	Two small MN tektite fragments were found at the top of the pebbly "laterite" layer. Ten fragments of MN tekitte with a total mass of 250 g were found on the surface of a quarry.	Fiske et al. 1999
7 km N of Khe Sahn	Vietnam	N16°40.71'	E106°42.33'	MN	86 MN tektite fragments with a total mass of 500 g were concentrated in the upper 10 cm of the pebbly quartzite clasts layer.	Fiske et al. 1999
~ 1 km S of Xeno	Laos	N16°39.6'	E105°00.5'	MN	Two MN tektite fragments with total weight of 3.9 g were found from a reddish "laterite" layer containing scattered quartz pebbles.	Schnetzler and McHone 1996
~ 9 km S of Xeno	Laos	N16°35.2'	E105°02.3'	MN	Four MN tektite fragments with total weight of 4.8 g were found from a reddish "laterite" layer containing scattered quartz pebbles.	Schnetzler and McHone 1996
~ 11 km of Xeno	Laos	N16°34.2'	E105°01.9'	MN	A MN tekitte fragment with weight of 3.0 g was found from a reddish "laterite" layer containing scattered quartz pebbles.	Schnetzler and McHone 1996
Ban Fang	Thailand	N16°27.83'	E102°37.83'	Not described	One tektite is from the upperpart of the "laterite layer", ~1.2 m below the surface.	Tamura, 1992
Khon Kaen University	Thailand	N16°28.83'	E102°49.91'	Not described	One tektite is from the upperpart of the "laterite layer", ~1.2 m below the surface.	Tamura, 1992
Ban Non Chai	Thailand	N16°22.83'	E102°51.45'	Not described	One tektite is from the "laterite layer", partly exposed in the ground surface.	Tamura, 1992
Ban Samran	Thailand	N16°32.73'	E102°49.85'	Not described	One tektite is from the "laterite layer", partly exposed in the ground surface.	Tamura, 1992
Ban Khan Kaem Khun	Thailand	N16°40.50'	E102°48.33'	Not described	One tektite is from the "laterite layer", partly exposed in the ground surface.	Tamura, 1992
Noen Sa-nga	Thailand	N15°36.50'	E101°58.00'	Irregular shape	A small piece of irregular shaped tektite with weight of 8.75 g is found at the top of the "laterite" layer.	Songtham et al. 2011; 2012
Gongpozhen*	Hainan (China)	N19°47.24'	E110°48.30'	Sp. and Irregular shape	Several pieces of Sp. and irregular shaped tektite were found at the top of a sandy gravel layer, several tens of centimeters below the surface (detail was not provided).	Lin and Uda, 1997
Qionhai*	Hainan (China)	N19°19.13'	E110°31.12'	Sp. and Irregular shape	Several pieces of Sp. and irregular shaped tektite were found at the top of a sandy gravel layer, several tens of centimeters below the surface (detail was not provided).	Lin and Uda, 1997
Sanya*	Hainan (China)	N18°26.44'	E109°29.40'	MN	Twenty tektiets (at least one of them was MN type) were found from a unconlidated sediments (detail was not provided).	Shimo et al. 2010

*Approximate site location from sketch map and name assigned from a nearby village

MN: Muong Nong-type, Sp: splash form

Table 2.2 Major element compositions of the MN tektite fragments from the HO06 section

Sample	SiO_2 (1σ)	Al_2O_3 (1σ)	MgO (1σ)	FeO (1σ)	CaO (1σ)	Na_2O (1σ)	K_2O (1σ)	MnO (1σ)	TiO_2 (1σ)	Total (1σ)
HO06MN16	79.29 (1.30)	9.64 (0.62)	1.25 (0.14)	3.63 (0.29)	1.10 (0.15)	1.01 (0.07)	2.27 (0.10)	0.09 (0.06)	0.56 (0.08)	98.84 (0.53)
HO06MN79	78.52 (2.90)	10.29 (1.76)	1.46 (0.31)	3.70 (0.58)	1.00 (0.19)	1.03 (0.14)	2.27 (0.09)	0.08 (0.05)	0.62 (0.08)	98.97 (0.62)
HO06MN105	79.56 (1.25)	9.72 (0.85)	1.37 (0.18)	3.61 (0.32)	0.89 (0.14)	0.96 (0.12)	2.30 (0.13)	0.07 (0.05)	0.61 (0.06)	99.11 (0.45)
HO06MN119	80.18 (1.27)	9.19 (0.93)	1.20 (0.13)	3.45 (0.40)	1.21 (0.08)	0.97 (0.08)	2.13 (0.14)	0.09 (0.06)	0.58 (0.05)	99.01 (0.59)
HO06MN121	79.46 (1.02)	9.86 (0.74)	1.37 (0.10)	3.58 (0.20)	1.14 (0.07)	0.92 (0.06)	2.34 (0.08)	0.11 (0.07)	0.58 (0.04)	99.36 (0.53)
HO06MN122	79.6 (1.07)	9.46 (0.64)	1.33 (0.09)	3.44 (0.32)	1.17 (0.13)	0.98 (0.06)	2.17 (0.19)	0.10 (0.07)	0.55 (0.07)	98.85 (0.51)
HO06MN124	79.54 (0.80)	9.59 (0.60)	1.14 (0.09)	3.48 (0.29)	0.80 (0.04)	1.03 (0.05)	2.27 (0.11)	0.10 (0.06)	0.56 (0.08)	98.51 (0.43)
HO06MN129	79.36 (1.13)	9.61 (0.56)	1.22 (0.19)	3.50 (0.38)	1.19 (0.09)	1.00 (0.05)	2.31 (0.10)	0.11 (0.07)	0.57 (0.06)	98.86 (0.57)
HO06MN141	79.17 (1.33)	9.87 (0.90)	1.22 (0.16)	3.52 (0.28)	0.86 (0.10)	0.98 (0.07)	2.32 (0.05)	0.10 (0.04)	0.63 (0.07)	98.69 (0.25)
Average	79.41 (0.42)	9.69 (0.29)	1.29 (0.10)	3.55 (0.09)	1.04 (0.15)	0.99 (0.03)	2.27 (0.07)	0.10 (0.01)	0.58 (0.03)	98.91 (0.23)
Koeberl 1992 (n=19)	78.95 (1.52)	10.19 (0.98)	1.43 (0.13)	3.75 (0.35)	1.21 (0.15)	0.92 (0.09)	2.42 (0.10)	0.08 (0.01)	0.63 (0.05)	99.59 (0.25)
Fiske et al. 1996 (n=3)	79.83 (0.15)	9.11 (0.15)	1.51 (0.03)	3.39 (0.04)	1.46 (0.03)	1.52 (0.04)	2.27 (0.02)	0.09 (0.00)	0.61 (0.01)	99.78 (0.24)
Herzog et al. 2008 (n=2)	78.56 (0.35)	11.02 (0.19)	1.71 (0.01)	4.10 (0.06)	1.65 (0.01)	0.80 (0.03)	2.45 (0.01)	0.07 (0.03)	0.70 (0.01)	101.05 (0.06)
Glass and Koeberl 1989 (n=1)	79.2	10.3	1.41	3.76	1.09	0.87	2.44	0.09	0.62	99.78

Chapter 3

Discovery of Shocked Quartz from the Quaternary Sequence at Huai Om section, Northeastern Thailand

This chapter is not available for publication because it is scheduled to be published in a journal within five years.

本章については、5 年以内に雑誌等で刊行予定のため、非公開

Chapter 4

Distribution of the Ejecta-bearing Sequence: The Results of the Field Survey across Eastern Indochina

This chapter is not available for publication because it is scheduled to be published in a journal within five years.

本章については、5 年以内に雑誌等で刊行予定のため、非公開

Chapter 5

General Discussion: Identification and Depositional Process of the Ejecta Deposit and Implication for the Location, Magnitude, and Target Rocks of the Impact

This chapter is not available for publication because it is scheduled to be published in a journal within five years.

本章については、5 年以内に雑誌等で刊行予定のため、非公開

Chapter 6
Conclusion

This thesis attempted to identify the on-land ejecta deposit in the Indochina Peninsula derived from the AATE and to clarify its lithostratigraphy, distribution, and depositional process for a better understanding of the nature of the AATE.

In Chapter **2,** I reported a detailed occurrence of tektite fragments found within the "laterite" layer at the HO06 section located in Ubon Ratchathani province, northeastern Thailand, and demonstrated that the tektite fragments in the "laterite" layer are of primary depositional origin. The very angular shapes and very poor sorting of the fragments, similar chemical composition of the fragments, restoration of a part of the original MN tektite mass, and the CT scan analysis revealed that the tektite fragments were formed by fragmentation of one large MN tektite mass at the time of its landing after the ejection by the impact, and has not been disturbed further (i.e., in situ). This result is contrary to the previous interpretation that similar tektite fragments were reworked on the upper surface of the "laterite" layer, which was interpreted as the paleo-erosional surface (Fiske et al. 1996), and indicates that the "laterite" layer is a part of the ejecta layer derived from the AATE.

In Chapter 3, I reported detailed lithostratigraphy of the Quaternary sequence including the "laterite" layer, and discovery of the shocked quartz grains with planar deformation features (PDFs) throughout the Quaternary sequence at Huai Om section in Ubon Ratchathani province, northeastern Thailand. The Quaternary sequence can be divided into three lithostratigraphic units (Units 1-3 in ascending order). Shocked quartz grains with PDFs were found throughout Units 1-3. PDFs were identified based on observation under an optical microscope, measurement of their orientation with a universal stage microscope, and further observations under SEM and TEM. This is the first report that shocked quartz with PDFs was identified from the Quaternary deposits in Indochina, and the result strongly indicates that Units 1-3 in this locality compose one sequence of the ejecta deposit.

In Chapter **4,** I reported the lithostratigraphy of the Quaternary sequence for seven representative sites selected from 20 studied sites across eastern Indochina (northeastern Thailand, southern Laos, northern Cambodia, and central Vietnam) to investigate the distribution of the ejecta-bearing sequence described in Chapters **2** and **3**. Basically, the

same lithostratigraphic units (Units 1-3) are observed at these sites.

Unit 1 is composed of gravel-bearing silt to sand layers or a gravel layer containing materials reworked from the local basement. The thickness of Unit 1 is about 30 cm to 2 m. This unit is not laterally continuous and absent at many localities. Unit 2 is composed of a very poorly-sorted breccia layer corresponding to the "laterite" layer. The thickness of Unit 2 is about 30 cm to more than 9 m, and thinner in northeastern Thailand and northern Cambodia, and thicker in southwestern Laos. The size of the gravels tends to be smaller in northeastern Thailand and northern Cambodia (2-4 mm), and larger in southern Laos (1-8 cm). The gravels are composed mainly of heavily weathered basalt fragments and red sandstone and mudstone fragments at sites in southern Laos. On the other hand, the gravels are composed mainly of white quartzite fragments with a minor presence of red sandstone and mudstone fragments at sites in northeastern Thailand and northern Cambodia. Tektites (both splash-form and MN tektite fragments) were found from the top of or within the upper part of this unit at several sites. Unit 3 is composed of a well-sorted silt to sand layer. Although the original thickness of this unit is unknown because this unit is truncated and covered by modern soil, the observed thickness of Unit 3 is various from site to site, about 30 cm to 3 m.

In Chapter 5, the depositional process of the ejecta-bearing quaternary sequence (Units 1-3) and implications for the location, magnitude, and target rocks of the AATE are discussed based on the lithostratigraphy, spatial distributions of the thickness and the grain size, and types of gravels in the ejecta deposit.

Based on their stratigraphic position and lithological and sedimentological evidence, Units 1-3 are interpreted as deposits formed by the following processes: rework of the local basement rocks by the impact-generated wind loaded with fine ejecta (Unit 1), followed by deposition of the ejecta curtain materials including gravels derived from the target rocks and tektites (Unit 2), and finally deposition of fallout fine ejecta (Unit 3).

The thickness of Unit 2 becomes thicker toward southwestern Laos. This thickness distribution of Unit 2, as well as the fact that the size of gravels in Unit 2 becomes larger toward southwestern Laos, indicates that the location of the impact is somewhere in southwestern Laos. The regression analysis of the thickness distribution of Unit 2 under the assumption that the log thickness is negatively correlated with log distance from the source area indicates that the Bolavean Plateau area (15.2°N, 106.1°E) is the most probable impact site of the AATE. This result strongly supports the hypothesis

of Sieh et al. (2019) that the AATE occurred in the basalt field of Bolaven Plateau, and the crater was buried by younger basalts that erupted after the impact.

The presence of the weathered basalt fragments, sandstone and mudstone fragments, and fragments of rounded quartzite gravels in Unit 2 indicates that the target rock of the AATE includes basalt, Mesozoic sedimentary basement rocks, and possibly Quaternary river gravels. This further supports the hypothesis of Sieh et al. (2019).

To establish the distribution of the ejecta layer of AATE and to better constrain the impact site, crater size, impact angle, and impact orientation, it will be needed to conduct additional field surveys on the ejecta layer in Bolaven Plateau close to the estimated impact site, and in southern Vietnam and northern Laos, that are the area further away from the estimated impact site.

In order to confirm the existence of the AATE crater under the basalt in the Bolavan Plateau, it will be required to conduct drilling through the basalt layer and recover rock samples to investigate the presence of impact-derived rocks such as impact breccia, suevite, and melt rock.

Since the ejecta deposit reported in this thesis is the youngest for large impact events on Earth, detailed investigation on vertical and lateral variations of the degree of shock deformation of ejecta materials at multiple sites in Indochina will provide information for understanding the process of ejecta dispersion due to large impacts on Earth.

Acknowledgments

This study was carried out under the guidance of supervisors Prof. E. Tajika and Emeritus professor R. Tada of the Department of Earth and Planetary Science, the University of Tokyo. Emeritus Professor P. A. Carling of the Southampton University, Prof. W. Songtham of the Nakhon Ratchasima Rajabhat University, and Prof. Lê Xuân Thuyên of the Vietnam National University Ho Chi Minh City University of Science, are greatly thanked for a lot of comments and discussions, and their support in the field. I am deeply thankful for their assistance in all aspects of this research. Prof. K. Goto, Prof. A. Kano, Prof. S. Sugita, and Associate Prof. M. Ikeda reviewed this thesis and gave me helpful and constructive comments, which improved this thesis. I am deeply indebted to P. Chansom of the Nakhon Ratchasima Rajabhat University for his extremely powerful support and long driving in the field. He was most adept at searching tektites in the field. I sincerely thank P. Jintasakul, the director of Khorat Fossil Museum, and P. Singhwachiraworakul for their hospitality during the field survey. I would also like to thank J. Yoshioka of the University of Tokyo for his support in the field. I wish to thank Y. Chang of the University of Tokyo for his help in identifying shocked quartz. I wish to express my sincere gratitude to Prof. T. Kogure of the University of Tokyo for his guidance and support on the SEM/TEM observations. I am obliged to W. Tarora to conduct the sample preparation with FIB for TEM observation. I am grateful to Dr. H. Yoshida of the University of Tokyo for his help in electron microprobe analyses. I am much obliged to Dr. C. Sakata and Dr. M. Makoto to conduct CT scanning of the block sample. I am grateful to Dr. T. Tsuihiji, S. Tada, A. Mizukami, N. Wakimizu, K. Yoshizawa, and H. Ueda of the University of Tokyo for their kind help on the analysis of the CT scan images. I sincerely thank Dr. K. Kurosawa of the Chiba Institute of Technology for valuable discussions. I thank members of the Hyousou seminar for their comments and discussion. I also thank Dr. H. Tuffen of Lancaster University for his kind help during my visit to Lancaster University. I sincerely appreciate Dr. S. Muto and K. Yoshizawa for their great help and kindness during my undergraduate, master's, and doctoral programs.

References

Abramoff, M.D., Magalhães, P.J., Ram, S.J., 2004. Image Processing with ImageJ. Biophotonics Int. 11, 36–42. https://doi.org/10.1201/9781420005615.ax4

Alexopoulos, J.S., Grieve, R.A.F., Robertson, R.B., 1988. Microscopic lamellar deformation features in quartz: Discriminative characteristics of shock-generated varieties. Geology 16, 796–799.

Alvarez, L.W., Alvarez, W., Asaro, F., Michel, H. V., 1980. Extraterrestrial cause for the Cretaceous-Tertiary extinction. Science (80-.). 298, 1095–1108.

Alvarez, W., Claeys, P., Kieffer, S.W., 1995. Emplacement of cretaceous-tertiary boundary shocked quartz from chicxulub crater. Science 269, 930–935. https://doi.org/10.1126/science.269.5226.930

Ashworth, J.R., Schneider, H., 1985. Deformation and transformation in experimentally shock-loaded quartz. Phys. Chem. Miner. 11, 241–249. https://doi.org/10.1007/BF00307401

Barnes, V.E., Pitakpaivan, K., 1962. Origin Of Indochinite Tektites. Proc Natl Acad Sci 48, 947–955.

Becker, L., Poreda, R.J., Basu, A.R., Pope, K.O., Harrison, T.M., Nicholson, C., Iasky, R., 2004. Bedout : A Possible End-Permian Impact Crater Offshore of Northwestern Australia. Science (80-.). 304, 1469–1476.

Bjørk, T.E., Mair, K., Austrheim, H., 2009. Quantifying granular material and deformation: Advantages of combining grain size, shape, and mineral phase recognition analysis. J. Struct. Geol. 31, 637–653. https://doi.org/10.1016/j.jsg.2009.03.020

Blum, J.D., Papanastassiou, D.A., Koeberl, C., Wasserburg, G.J., 1992. Neodymium and strontium isotopic study of Australasian tektites: New constraints on the provenance and age of target materials. Geochim. Cosmochim. Acta 56, 483–492. https://doi.org/10.1016/0016-7037(92)90146-A

Booth, J., Sattayarak, N., 2011. Subsurface Carboniferous – Cretaceous geology of NE Thailand, in: Ridd, M.F., Barber, A.J., Crow, M.J. (Eds.), The Geology of Thailand. Geological Society, London, pp. 185–222. https://doi.org/10.1144/goth.9

Bunopas, S., Wasson, J.T., Vella, P., Fortaine, H., Hada, S., Burrett, C.F., Suphajunya, T., Khositanont, S., 1999. Catastrophic loess, mass mortality and forest fires suggest that a Pleistocene cometary impact in Thailand caused the Australasian Tektite Field. J. Geol. Soc. Thail. 1, 1–17.

Campanale, F., Mugnaioli, E., Folco, L., Gemmi, M., Lee, M.R., Daly, L., Glass, B.P., 2019. Evidence for subsolidus quartz-coesite transformation in impact ejecta from the Australasian tektite strewn field. Geochim. Cosmochim. Acta 264, 105–117. https://doi.org/10.1016/j.gca.2019.08.014

Capaccioni, F., Cerroni, P., Coradini, M., Di Martino, M., Farinella, P., Flamini, E., Martelli, G., Paolicchi, P., Smith, P.N., Woodward, A., Zappala, V., 1986. Asteroidal catastrophic collisions simulated by hypervelocity impact experiments. Icarus 66, 487–514. https://doi.org/10.1016/0019-1035(86)90087-4

Capaccioni, F., Cerroni, P., Coradini, M., Farinella, P., Flamini, E., Martelli, G., Paolicchi, P., Smith, P.N., Zappala, V., 1984. Shapes of asteroids compared with fragments from hypervelocity impact experiments. Nature 308, 832–834. https://doi.org/10.1038/308832a0

Carr, M.H., Crumpler, L.S., Cutts, J.A., Greeley, R., Guest, J.E., Masursky, H., 1977. Martian impact craters and emplacement of ejecta by surface flow. J. Geophys. Res. 82, 4055–4065. https://doi.org/10.1029/js082i028p04055

Cavosie, A.J., Koeberl, C., 2019. Overestimation of threat from 100 Mt-class airbursts? High-pressure evidence from zircon in Libyan Desert Glass. Geology 47, 609–612. https://doi.org/10.1130/G45974.1

Cavosie, A.J., Timms, N.E., Erickson, T.M., Koeberl, C., 2018. New clues from Earth's most elusive impact crater: Evidence of reidite in Australasian tektites from Thailand. Geology 46, 203–206. https://doi.org/10.1130/G39711.1

Chang, Y., 2018. Depositional processes of impactites from the YAX-1 drill core in the Chicxulub impact structure inferred from vertical profiles of PDF orientations and grain size distributions of shocked quartz. Meteorit. Planet. Sci. 1–18. https://doi.org/10.1111/maps.13082

Chao, E.C.T., 1967. Shock effects in certain rock-forming minerals. Science (80-.). 156, 192–202. https://doi.org/10.1126/science.156.3772.192

Choowong, M., 2011. Quaternaly, in: Ridd, M.F., Barber, A.J., Crow, M.J. (Eds.), The Geology of Thailand. Geological Society, London, pp. 335–350.

Christie, J.M., Ardell, A.J., 1974. Substructures of deformation lamellae in quartz. Geology 2, 405–408. https://doi.org/10.1130/0091-7613(1974)2<405:SODLIQ>2.0.CO;2

Christie, J.M., Griggs, D.T., Carter, N.L., 1964. Experimental evidence of basal slip in quartz. J. Geol. 72, 734–756.

Christie, J.M., Raleigh, C.B., 1959. The origin of deformation lamellae in quartz. Am. J. Sci. 257, 385–407. https://doi.org/10.2475/ajs.257.6.385

Collins, G.S., Melosh, J., Marcus, R.A., 2005. Earth Impact Effects Program: A Web-based computer program for calculating the regional environmental consequences of a meteoroid impact on Earth. Meteorit. Planet. Sci. 40, 817. https://doi.org/10.1111/j.1945-5100.2005.tb00157.x

Cordier, P., Doukhan, J.-C., 1989. Water solubility in quartz and its influence on ductility. Eur. J. Mineral. 1, 221–238. https://doi.org/10.1127/ejm/1/2/0221

Cordier, P., Vrána, S., Doukhan, J.C., 1994. Shock metamorphism in quartz at Sevetin and Susice (Bohemia)? A TEM investigation. Meteoritics 29, 98–99. https://doi.org/10.1111/j.1945-5100.1994.tb00660.x

Cox, M.A., Cavosie, A.J., Ferrière, L., Timms, N.E., Bland, P.A., Miljković, K., Erickson, T.M., Hess, B., 2019. Shocked quartz in polymict impact breccia from the Upper Cretaceous Yallalie impact structure in Western Australia. Meteorit. Planet. Sci. 54, 621–637. https://doi.org/10.1111/maps.13238

Crosta, G.B., Frattini, P., Fusi, N., 2007. Fragmentation in the Val Pola rock avalanche, Italian Alps. J. Geophys. Res. Earth Surf. 112, 1–23. https://doi.org/10.1029/2005JF000455

Demeter, F., Patole-Edoumba, E., Duringer, P., Bacon, A.M., Sytha, P., Bano, M., Laychour, V., Cheangleng, M., Sari, V., 2010. Reinterpretation of an archaeological pebble culture from the Middle Mekong River valley, Cambodia. Geoarchaeology 25, 75–95. https://doi.org/10.1002/gea.20298

Derez, T., Pennock, G., Drury, M.R., Sintubin, M., 2016. Three sets of crystallographic sub-planar structures in quartz formed by tectonic deformation. Earth Planet. Sci. Lett. 442, 157–161. https://doi.org/10.1016/j.epsl.2016.03.005

Domokos, G., Kun, F., Sipos, A.A., Szabo, T., 2015. Universality of fragment shapes. Sci. Rep. 5, 1–6. https://doi.org/10.1038/srep09147

Drury, M.R., 1993. Deformation lamellae in metals and minerals, in: Boland, J.N., Fitz

Gerald, J.D. (Eds.), Defects and Processes in the Solid State: Geoscience Applications. Elsevier, Amsterdam, pp. 195–212.

Engelhardt, W. Von, Bertsch, W., 1969. Shock induced planar deformation structures in quartz from the Ries crater, Germany. Contrib. to Mineral. Petrol. 20, 203–234. https://doi.org/10.1007/BF00377477

Ernstson, K., Fiebag, J., 1992. The Azuara impact structure (Spain): new insights from geophysical and geological investigations. Geol. Rundschau 81, 403–427. https://doi.org/10.1007/BF01828607

Farris, D.W., Paterson, S.R., 2007. Contamination of silicic magmas and fractal fragmentation of xenoliths in Paleocene plutons on Kodiak Island, Alaska. Can. Mineral. 45, 107–129. https://doi.org/10.2113/gscanmin.45.1.107

Fassett, C. I., Head, J. W., Smith, D. E., Zuber, M. T., Neumann, G. A., 2011. Thickness of proximal ejecta from the Orientale Basin from Lunar Orbiter Laser Altimeter (LOLA) data: Implications for multi‐ring basin formation. Geophysical Research Letters, 38(17).

Fedorov, P.I., Koloskov, A. V., 2005. Cenozoic volcanism of Southeast Asia. Petrology 13, 352–380.

Ferrière, L., Morrow, J.R., Amgaa, T., Koeberl, C., 2009. Systematic study of universal-stage measurements of planar deformation features in shocked quartz : Implications for statistical significance and representation of results. Meteorit. Planet. Sci. 940, 925–940.

Fiske, P.S., Putthapiban, P., Wasson, J.T., 1996. Excavation and analysis of layered tektites from northeast Thailand: Results of 1994 field expedition. Meteorit. Planet. Sci. 31, 36–41.

Fiske, P.S., Schnetzlerz, C., Mchone, J., Kham, K., 1999. Layered tektites of southeast Asia : Field studies in central Laos and Vietnam. Meteorit. Planet. Sci. 34, 757–761.

Folco, L., Bigazzi, G., Orazio, M.D., Balestrieri, M.L., 2011. Fission track age of Transantarctic Mountain microtektites. Geochim. Cosmochim. Acta 75, 2356–2360. https://doi.org/10.1016/j.gca.2011.02.014

Folco, L., D'Orazio, M., Gemelli, M., Rochette, P., 2016. Stretching out the Australasian microtektite strewn field in Victoria Land Transantarctic Mountains. Polar Sci. 10, 147–159. https://doi.org/10.1016/j.polar.2016.02.004

Folco, L, Glass, B.P., Orazio, M.D., Rochette, P., 2018. ScienceDirect Australasian microtektites : Impactor identification using Cr , Co and Ni ratios. Geochim. Cosmochim. Acta 222, 550–568. https://doi.org/10.1016/j.gca.2017.11.017

Folco, L., Mugnaioli, E., Gemelli, M., Masotta, M., Campanale, F., 2018. Direct quartz-coesite transformation in shocked porous sandstone from Kamil Crater (Egypt). Geology 46, 739–742. https://doi.org/10.1130/G45116.1

Folco, L., Perchiazzi, N., Orazio, M.D., Frezzotti, M.L., Glass, B.P., Rochette, P., Nazionale, M., Siena, U., Laterina, V., Pisa, U., Maria, V.S., 2010. Shocked quartz and other mineral inclusions in Australasian microtektites 211–214. https://doi.org/10.1130/G30512.1

Folk, R.L., Ward, W., 1957. Brazos river bar; a study in the significance of grain size parameters. J Sediment Petorol 27, 3–26.

Ford, R.J., 1988. An empirical model for the Australasian tektite field. Aust. J. Earth Sci. 35, 483–490. https://doi.org/10.1080/08120098808729464

French, B.M., Cordua, W.S., Plescia, J.B., 2004. The Rock Elm meteorite impact structure, Wisconsin: Geology and shock-metamorphic effects in quartz. Bull. Geol. Soc. Am. 116, 200–218. https://doi.org/10.1130/B25207.1

French, B.M., Koeberl, C., 2010. The convincing identification of terrestrial meteorite impact structures: What works, what doesn't, and why. Earth-Science Rev. 98, 123–170. https://doi.org/10.1016/j.earscirev.2009.10.009

French, B.M., Underwood, J.R., Edward, P.F., 1974. Shock-metamorphic features in two meteorite impact structures, southeastern Libya. Bull. Geol. Soc. Am. 85, 1425–1428. https://doi.org/10.1130/0016-7606(1974)85<1425:SFITMI>2.0.CO;2

Fudali, R.F., Dyar, M.D., Griscom, D.L., Schreiber, H.D., 1987. The oxidation state of iron in tektite glass. Geochim. Cosmochim. Acta 51, 2749–2756. https://doi.org/10.1016/0016-7037(87)90154-2

Fujiwara, A., Kamimoto, G., Tsukamoto, A., 1978. Expected shape distribution of asteroids obtained from laboratory impact experiments. Nature 272, 602–603.

Glasmann, J.R., Simonson, G.H., 1985. Alteration of basalt in soils of western Oregon. Soil Sci. Soc. Am. J. 49, 262–273.

Glass, B.P., Barlow, R.A., 1979. Mineral inclusions in Muong Nong‐type indochinites: Implications concerning parent material and process of formation. Meteoritics 14, 55–67.

Glass, B.P., Folco, L., Masotta, M., Campanale, F., 2020. Coesite in a Muong Nong-type tektite from Muong Phin, Laos: Description, formation, and survival. Meteorit. Planet. Sci. 55, 253–273. https://doi.org/10.1111/maps.13433

Glass, B.P., Jiquan Wu, 1993. Coesite and shocked quartz discovered in the Australasian and North American microtektite layers. Geology 21, 435–438. https://doi.org/10.1130/0091-7613(1993)021<0435:CASQDI>2.3.CO;2

Glass, B.P., Koeberl, C., 2006. Australasian microtektites and associated impact ejecta in the South China Sea and the Middle Pleistocene supereruption of Toba. Meteorit. Planet. Sci. 41, 305–326.

Glass, B.P., Koeberl, C., 1989. Trace element study of high- and low-refractive index Muong Nong-type tektites from Indochina. Meteoritics 24, 143–146. https://doi.org/10.1111/j.1945-5100.1989.tb00956.x

Glass, B.P., Pizzuto, J.E., 1994. Geographic variation in Australasian microtektite concentrations: Implications concerning the location and size of the source crater. J. Geophys. Res. 99, 19075. https://doi.org/10.1029/94JE01866

Glass, B.P., Simonson, B.M., 2012. Distal impact ejecta layers: Spherules and more. Elements 8, 43–48. https://doi.org/10.2113/gselements.8.1.43

Glikson, A., 2004. Comment on "Bedout: a possible end-Permian impact crater offshore of Northwestern Australia". Science (80-.). 306. https://doi.org/10.1126/science.1100404

Goltrant, O., Cordier, P., Doukhan, J.C., 1991. Planar deformation features in shocked quartz; a transmission electron microscopy investigation. Earth Planet. Sci. Lett. 106, 103–115. https://doi.org/10.1016/0012-821X(91)90066-Q

Goltrant, O., Leroux, H., Doukhan, J.C., Cordier, P., 1992. Formation mechanisms of planar deformation features in naturally shocked quartz. Phys. Earth Planet. Inter. 74, 219–240. https://doi.org/10.1016/0031-9201(92)90012-K

Gratz, A.J., Fisler, D.K., Bohor, B.F., 1996. Distinguishing shocked from tectonically deformed quartz by the use of the SEM and chemical etching. Earth Planet. Sci. Lett. 142, 513–521.

Gratz, A.J., Nellis, W.J., Christie, J.M., Brocious, W., Swegle, J., Cordier, P., 1992. Shock Metamorphism of Quartz with Initial temparatures -170 to +1000°C. Phys. Chem. Miner. 19, 267−288.

Greenland, L.P., Lovering, J.F., 1962. Selective Volatilization from Tektites. Nature 196,

1195–1196. https://doi.org/10.1038/1961195a0

Grieve, R.A.F., Langenhorst, F., Stöffler, D., 1996. Shock metamorphism of quartz in nature and experiment: II. Significance in geoscience. Meteorit. Planet. Sci. 31, 6–35. https://doi.org/10.1111/j.1945-5100.1996.tb02049.x

Grieve, R.A.F., Robertson, R.B., 1976. Variations in shock deformation at the Slate Islands impact structure, Lake Superior, Canada. Contrib. to Mineral. Petrol. 58, 37–49. https://doi.org/10.1007/BF00384743

Haines, P.W., Howard, K.T., Ali, J.R., Burrett, C.F., Bunopas, S., 2004. Flood deposits penecontemporaneous with ~0.8 Ma tektite fall in NE Thailand: Impact-induced environmental effects? Earth Planet. Sci. Lett. 225, 19–28. https://doi.org/10.1016/j.epsl.2004.05.008

Hamers, M.F., Drury, M.R., 2011. Scanning electron microscope-cathodoluminescence (SEM-CL) imaging of planar deformation features and tectonic deformation lamellae in quartz. Meteorit. Planet. Sci. 46, 1814–1831. https://doi.org/10.1111/j.1945-5100.2011.01295.x

Hasegawa, H., Imsamut, S., Charusiri, P., Tada, R., Horiuchi, Y., Hisada, K.I., 2010. “Thailand was a desert” during the mid-Cretaceous: Equatorward shift of the subtropical high-pressure belt indicated by eolian deposits (Phu Thok Formation) in the Khorat Basin, northeastern Thailand. Isl. Arc 19, 605–621. https://doi.org/10.1111/j.1440-1738.2010.00728.x

Herzog, G.F., Alexander, C.M.O.D., Berger, E.L., Delaney, J.S., Glass, B.P., 2008. Potassium isotope abundances in Australasian tektites and microtektites. Meteorit. Planet. Sci. 43, 1641–1657. https://doi.org/10.1111/j.1945-5100.2008.tb00634.x

Howard, K.T., Bunopas, S., Burrett, C.F., Haines, P.W., Norman, M.D., 2000. THE 770KA TEKTITE PRODUCING IMPACT EVENT: EVIDENCE FOR DISTAL ENVIRONMENTAL EFFECTS IN NE THAILAND, in: 31st Lunar and Planetary Science Conference. p. abstract #1308.

Hyodo, M., Matsu, S., Kamishima, Y., Kondo, M., Takeshita, Y., Kitaba, I., 2011. High-resolution record of the Matuyama – Brunhes transition constrains the age of Javanese Homo erectus in the Sangiran dome , Indonesia. https://doi.org/10.1073/pnas.1113106108

Jébrak, M., 1997. Hydrothermal breccias in vein-type ore deposits: A review of mechanisms, morphology and size distribution. Ore Geol. Rev. 12, 111–134.

https://doi.org/10.1016/S0169-1368(97)00009-7

Joreau, P., French, B.M., Doukhan, J.C., 1996. A TEM investigation of shock metamorphism in quartz from the Sudbury impact structure (Canada). Earth Planet. Sci. Lett. 138, 137–143. https://doi.org/10.1016/0012-821x(95)00236-6

Jourdan, F., Nomade, S., Wingate, M.T.D., Eroglu, E., Deino, A., 2019. Ultraprecise age and formation temperature of the Australasian tektites constrained by 40Ar/39Ar analyses. Meteorit. Planet. Sci. 54, 2573–2591. https://doi.org/10.1111/maps.13305

Keates, S.G., 2000. Tektites and the Age Paradox in Mid-Pleistocene China. Science (80-.). 289, 507a.

Kenkmann, T., Deutsch, A., Thoma, K., Ebert, M., Poelchau, M.H., Buhl, E., Carl, E.R., Danilewsky, A.N., Dresen, G., Dufresne, A., Durr, N., Ehm, L., Grosse, C., Gulde, M., Güldemeister, N., Hamann, C., Hecht, L., Hiermaier, S., Hoerth, T., Kowitz, A., Langenhorst, F., Lexow, B., Liermann, H.P., Luther, R., Mansfeld, U., Moser, D., Raith, M., Reimold, W.U., Sauer, M., Schäfer, F., Schmitt, R.T., Sommer, F., Wilk, J., Winkler, R., Wünnemann, K., 2018. Experimental impact cratering: A summary of the major results of the MEMIN research unit. Meteorit. Planet. Sci. 53, 1543–1568. https://doi.org/10.1111/maps.13048

Kieffer, S.W., 1971. Metamorphism of the Coconino Sandstone at Meteor Crater , Arizona 76, 5449–5473.

Klein, L.C., Yinnon, H., Uhlmann, D.R., 1980. Viscous flow and crystallization behavior of tektite glasses. J. Geophys. Res. 85, 5485. https://doi.org/10.1029/jb085ib10p05485

Koeberl, C., 1994. Tektite origin by hypervelocity asteroidal or cometary impact, in: Dressler, B.O., Grieve, R.A.F., Sharpton, V.L.. (Eds.), Large Meteorite Impacts and Planetary Evolution: Geological Society of America Special Paper 293. p. 133. https://doi.org/10.1130/SPE293-p133

Koeberl, C., 1992. Geochemistry and origin of Muong Nong-type tektites. Geochim. Cosmochim. Acta 56, 1033–1064.

Koeberl, C., 1990. The geochemistry of tektites: an overview. Tectonophysics 171, 405–422. https://doi.org/10.1016/0040-1951(90)90113-M

Koeberl, C., Glass, B.P., 2000. Tektites and the age paradox in mid-pleistocene china. Science 289, 507a. https://doi.org/10.1126/science.289.5479.507a

Kowitz, A., Guldemeister, N., Schmitt, R.T., Reimold, W.U., Wunnemann, K., Holzwarth, A., 2016. Revision and recalibration of existing shock classifications for quartzose rocks using low-shock pressure (2.5-20 GPa) recovery experiments and mesoscale numerical modeling. Meteorit. Planet. Sci. 51, 1741–1761. https://doi.org/10.1111/maps.12712

Krumbein, W.C., 1941. Measurement and Geological Significance of Shape and Roundness of Sedimentary Particles. J. Sediment. Petrol. 11, 64–72.

La Marche, P.H., Rauch, F., Landford, W.A., 1984. Reaction between water and tektite glass. J. Non. Cryst. Solids 67, 361–369. https://doi.org/10.1016/0022-3093(84)90161-3

Langbroek, M., 2015. Do tektites really date the bifaces from the Bose (Baise) Basin ,. J. Hum. Evol. 80, 175–178. https://doi.org/10.1016/j.jhevol.2014.06.019

Langenhorst, F., 2002. Shock metamorphism of some minerals: Basic introduction and microstructural observations. Bull. Czech Geol. Surv. 77, 265–282.

Langenhorst, F., 1994. Shock Experiments on Pre-Heated Alpha-Quartz and Beta-Quartz: II. X-Ray and TEM Investigations. Earth Planet. Sci. Lett. 128, 683–698.

Langenhorst, F., Deutsch, A., 1996. The Azuara and Rubielos structures, Spain: Twin impact craters or Alpine thrust systems? TEM investigations on deformed quartz disprove shock origin. Lunar Planet. Sci. Conf. Vol. 27. 1996. 725–726.

Langenhorst, F., Deutsch, A., 1994. Shock experiments on pre-heated α- and β-quartz: I. Optical and density data. Earth Planet. Sci. Lett. 125, 407–420. https://doi.org/10.1016/0012-821X(94)90229-1

Langenhorst, F., Kyte, F.T., Retallack, G.J., 2005. REEXAMINATION OF QUARTZ GRAINS FROM THE PERMIAN-TRIASSIC BOUNDARY SECTIONAT GRAPHITE PEAK, ANTARCTICA (abstract #2358). 36th Annu. Lunar Planet. Sci. Conf. Leag. City, Texas.

Lee, M.-Y., Wei, K.-Y., 2000. Australasian microtektites in the South China Sea and the West Philippine Sea: Implications for age, size, and location of the impact crater. Meteorit. Planet. Sci. 35, 1151–1155. https://doi.org/10.1111/j.1945-5100.2000.tb01504.x

Leroux, H., Doukhan, J.-C., 1993. Dynamic deformation of quartz in the landslide of Kofels, Austria. Eur. J. Mineral. 5, 893–902. https://doi.org/10.1127/ejm/5/5/0893

Leroux, H., Warme, J.E., Doukhan, J.C., 1995. Shocked quartz in the Alamo breccia, southern Nevada: evidence for a Devonian impact event. Geology 23, 1003–1006. https://doi.org/10.1130/0091-7613(1995)023<1003:SQITAB>2.3.CO;2

Li, H., Lotter, M., Kuman, K., Lei, L., 2020. Population dynamics during the Acheulean at ~ 0.8 Ma in East and Southeast Asia: Considering the influence of two geological cataclysms. Palaeogeogr. Palaeoclimatol. Palaeoecol. https://doi.org/10.1016/j.palaeo.2020.109927

Lin, A., Uda, S., 1997. Tektites and pseudotachylytes in Hainan Island, South China. J. Geol. Soc. Japan 103, XXIII-XXIV (in Japanese).

Lyons, J.B., Officer, C.B., Borella, P.E., Lahodynsky, R., 1993. Planar lamellar substructures in quartz. Earth Planet. Sci. Lett. 119, 431–440. https://doi.org/10.1016/0012-821X(93)90151-X

Ma, P., Aggrey, K., Tonzola, C., Schnabel, C., de Nicola, P., Herzog, G.F., Wasson, J.T., Glass, B.P., Brown, L., Tera, F., Middleton, R., Klein, J., 2004. Beryllium-10 in Australasian tektites: Constraints on the location of the source crater. Geochim. Cosmochim. Acta 68, 3883–3896. https://doi.org/10.1016/j.gca.2004.03.026

Mansfeld, U., Langenhorst, F., Ebert, M., Kowitz, A., Schmitt, R.T., 2017. Microscopic evidence of stishovite generated in low-pressure shock experiments on porous sandstone: Constraints on its genesis. Meteorit. Planet. Sci. 52, 1449–1464. https://doi.org/10.1111/maps.12867

Matsu'ura, S., Kondo, M., Danhara, T., Sakata, S., Iwano, H., Hirata, T., Kurniawan, I., Set iyabudi, E., Takeshita, Y., Hyodo, M., Kitaba, I., Sudo, M., Danhara, Y., Aziz, F., 2020. Age control of the first appearance datum for Javanese Homo erectus in the Sangiran area. Science (80-.). 367, 210–214.

McCall, G.J.H., 2001. Tektites in the Geologicaal Record showers of glass from the sky. The Geological Society London.

McGetchin, T.R., Settle, M., Head, J.W., 1973. RADIAL THICKNESS VARIATION IN IMPACT CRATER EJECTA: IMPLICATIONS FOR LUNAR BASIN DEPOSITS. Russ. J. Math. Phys. 20, 226–236. https://doi.org/10.1016/0012-821X(73)90162-3

McLaren, A.C., Cook, R.F., Hyde, S.T., Tobin, R.C., 1983. The mechanisms of the formation and growth of water bubbles and associated dislocation loops in synthetic quartz. Phys. Chem. Miner. 9, 79–94.

https://doi.org/10.1007/BF00308151

McLaren, A.C., Hobbs, B.E., 1972. Transmission electron microscope investigation of some naturally deformed quartzites, in: Al., H.C.H. et (Ed.), Flow and Fracture of Rocks. AGU, Washington, D. C, pp. 55–66.

McLaren, A.C., Retchford, J.A., Griggs, D.T., Christie, J.M., 1967. Transmission Electron Microscope Study of Brazil Twins and Dislacations Experimentally Produced in Natural Quartz. Phys. Status Solidi 19, 631–644. https://doi.org/10.1002/pssb.19670190216

McMillan, P., Jr, R.R., 1986. Hydroxyl sites in SiO2 glass: A note on infrared and Raman spectra. Am. Mineral. 71, 772–778.

Melosh, J., 1989. Impact cratering: a geologic process. Oxford University Press New York.

Michikami, T., Hagermann, A., Kadokawa, T., Yoshida, A., Shimada, A., Hasegawa, S., Tsuchiyama, A., 2016. Fragment shapes in impact experiments ranging from cratering to catastrophic disruption. Icarus 264, 316–330. https://doi.org/10.1016/j.icarus.2015.09.038

Minezaki, T., Hisada, K. ichiro, Hara, H., Kamata, Y., 2019. Tectono-stratigraphy of Late Carboniferous to Triassic successions of the Khorat Plateau Basin, Indochina Block, northeastern Thailand: Initiation of the Indosinian Orogeny by collision of the Indochina and South China blocks. J. Asian Earth Sci. 170, 208–224. https://doi.org/10.1016/j.jseaes.2018.10.020

Mizera, J., Randa, Z., Kamenik, J., 2016. On a possible parent crater for Australasian tektites: Geochemical, isotopic, geographical and other constraints. Earth-Science Rev. 154, 123–137. https://doi.org/10.1016/j.earscirev.2015.12.004

Montanari, A., Koeberl, C., 2000. Impact stratigraphy: the Italian record. Springer.

Morgan, J., Lana, C., Kearsley, A., Coles, B., Belcher, C., Montanari, S., Diaz-Martinez, E., Barbosa, A., Neumann, V., 2006. Analyses of shocked quartz at the global K-P boundary indicate an origin from a single, high-angle, oblique impact at Chicxulub. Earth Planet. Sci. Lett. 251, 264–279. https://doi.org/10.1016/j.epsl.2006.09.009

Nakano, Y., Goto, K., Matsui, T., Tada, R., Tajika, E., 2008. PDF orientations in shocked quartz grains around the Chicxulub crater. Meteorit. Planet. Sci. 43, 745–760. https://doi.org/10.1111/j.1945-5100.2008.tb00682.x

Negishi, Y., Goto, M., Tsuda, K., Vilayhack, S., Duangsurign, S., Phommakaysone, K., Watanabe, Y., Kobayashi, S., Shibata, Y., 2009. Geology and mineral resources of the Attapeu area in southern Laos. Resour. Geol. 59, 107–122.

Nichol, J.E., Nichol, D.W., 2015. Character and provenance of aeolian sediments in northeast Thailand. Aeolian Res. 19, 5–14. https://doi.org/10.1016/j.aeolia.2015.09.001

Nuchanong, T., Chaodumrong, P., Luengingkasoot, M., Burrett, C., Techawan, S., Silakul, T., Stokes, R.B., Raksaskulwong, M., Chotikanatis, P., Kraikhong, C., Subtavewung, P., Assavapatchara, S., Imsamut, S. (Eds.), 2014. Geology of Thailand. Bureau of Geological Survey, Department of Mineral Resources, Bangkok, Thailand. https://doi.org/10.1306/83d91696-16c7-11d7-8645000102c1865d

Ocampo, A.C., Pope, K.O., Fischer, A.G., 1996. Ejecta blanket deposits of the Chicxulub crater from Albion Island, Belize, in: The Cretaceous-Tertiary Event and Other Catastrophes in Earth History: Geological Society of America Special Paper 307. pp. 75–88. https://doi.org/10.1130/0-8137-2307-8.75

Onose, N., Hasegawa, S., Okudaira, K., 2011. Mass and shape distributions of fragments produced in impact disruptions for better understanding of inner structure of asteroids which may hit the Earth (in Japanese). Spaceguard Res. 3, 4–7.

Pierazzo, E., Artemieva, N., 2012. Local and global environmental effects of impacts on earth. Elements 8, 55–60. https://doi.org/10.2113/gselements.8.1.55

Pope, K.O., Ocampo, A.C., Fischer, A.G., Alvarez, W., Fouke, W., Webster, C.L., Vega, F.J., Smit, J., Fritsche, A.E., Claeys, P., 1999. Chicxulub impact ejecta from Albion Island , Belize. Earth Planet. Sci. Lett. 170, 351–364.

Prasad, M.S., Mahale, V.P., Kodagali, V.N., 2007. New sites of Australasian microtektites in the central Indian Ocean: Implications for the location and size of source crater. J. Geophys. Res. E Planets 112. https://doi.org/10.1029/2006JE002857

Quintana, S.N., Schultz, P.H., Horowitz, S.S., 2018. Experimental constraints on impact-induced winds. Icarus 305, 91–104. https://doi.org/10.1016/j.icarus.2017.12.042

Racey, A., Love, M.A., Canham, A.C., Goodall, J.G.S., Polachan, S., Jones, P.D., 1996. Stratigraphy and reservoir potential of the Mesozoic Khorat Group, NE Thailand - Part 1: Stratigraphy and Sedimentary Evolution. J. Pet. Geol. 19, 5–40.

Raksaskulwong, M., Monjai, D., 2007. Relationship Between the Mahasarakham Formation and High Terrace Gravels Along the Khon Kaen-Kalasin, in: International Conference on Geology of Thailand.

Rea, D.K., Janecek, T.R., 1981. Late cretaceous history of eolian deposition in the mid-pacific mountains, central North Pacific Ocean. Palaeogeogr. Palaeoclimatol. Palaeoecol. 36, 55–67. https://doi.org/10.1016/0031-0182(81)90048-1

Reimold, W.U., Crósta, A.P., Hasch, M., Kowitz, A., Hauser, N., Sanchez, J.P., Simões, L.S.A., de Oliveira, G.J., Zaag, P.T., 2019. Shock deformation confirms the impact origin for the Cerro do Jarau, Rio Grande do Sul, Brazil, structure. Meteorit. Planet. Sci. 54, 2384–2397. https://doi.org/10.1111/maps.13233

Reimold, W.U., Ferrière, L., Deutsch, A., Koeberl, C., 2014. Impact controversies: Impact recognition criteria and related issues. Meteorit. Planet. Sci. 49, 723–731. https://doi.org/10.1111/maps.12284

Retallack, G.J., Seyedolali, A., Krull, E.S., Holser, W.T., Ambers, C.P., Kyte, F.T., 1998. Search for evidence of impact at the Permian-Triassic boundary in Antarctica and Australia. Geology 26, 979–982. https://doi.org/10.1130/0091-7613(1998)026<0979:SFEOIA>2.3.CO;2

Robertson, R.B., Grieve, 1977. Shock attenuation at terrestrial impact structures, in: Roddy, D.J., Pepin, R.O., Merrill, R.B. (Eds.), Impact and Explosion Cratering. Pergamon Press (New York), pp. 687–702.

Rost, R., 1969. Sculpturing of Moldavites and the Problem of Micromoldavites. J Geophys Res 74, 6816–6824.

Roy, S.G., Johnson, S.E., Koons, P.O., Jin, Z., 2012. Fractal analysis and thermal-elastic modeling of a subvolcanic magmatic breccia: The role of post-fragmentation partial melting and thermal fracture in clast size distributions. Geochemistry, Geophys. Geosystems 13, 1–23. https://doi.org/10.1029/2011GC004018

Ruesch, O., Sefton-Nash, E., Vago, J.L., Küppers, M., Pasckert, J.H., Khron, K., Otto, K., 2020. In situ fragmentation of lunar blocks and implications for impacts and solar-induced thermal stresses. Icarus 336, 113431. https://doi.org/10.1016/j.icarus.2019.113431

Ruiz-Carulla, R., Corominas, J., 2020. Analysis of Rockfalls by Means of a Fractal Fragmentation Model. Rock Mech. Rock Eng. 53, 1433–1455. https://doi.org/10.1007/s00603-019-01987-2

Sanderson, D.C.W., Bishop, P., Houston, I., Boonsener, M., 2001. Luminescence characterisation of quartz-rich cover sands from NE Thailand. Quat. Sci. Rev. 20, 893–900. https://doi.org/10.1016/S0277-3791(00)00014-7

Schmieder, M., Kring, D.A., 2020. Earth's Impact Events through Geologic Time: A List of Recommended Ages for Terrestrial Impact Structures and Deposits. Astrobiology 20, 91–141. https://doi.org/10.1089/ast.2019.2085

Schneider, C.A., Rasband, W.S., Eliceiri, K.W., 2014. NIH Image to ImageJ: 25 years of image analysis. Agric. Eng. 44, 93–102. https://doi.org/10.1038/nmeth.2089

Schnetzler, C., 1992. Mechanism of Muong Nong-type tektite formation and speculation on the source of Australasian tektites. Meteoritics 165, 154–165.

Schnetzler, C.C., McHone, J.F., 1996. Source of Australasian tektites: Investigating possible impact sites in Laos. Meteorit. Planet. Sci. 31, 73–76.

Schulte, P., Alegret, L., Arenillas, I., Arz, J.A., Barton, P.J., Bown, P.R., Bralower, T.J., Christeson, G.L., Claeys, P., Cockell, C.S., Collins, G.S., Deutsch, A., Goldin, T.J., Goto, K., Grajales-Nishimura, J.M., Grieve, R.A.F., Gulick, S.P.S., Johnson, K.R., Kiessling, W., Koeberl, C., Kring, D.A., MacLeod, K.G., Matsui, T., Melosh, J., Montanari, A., Morgan, J. V., Neal, C.R., Nichols, D.J., Norris, R.D., Pierazzo, E., Ravizza, G., Rebolledo-Vieyra, M., Reimold, W.U., Robin, E., Salge, T., Speijer, R.P., Sweet, A.R., Urrutia-Fucugauchi, J., Vajda, V., Whalen, M.T., Willumsen, P.S., 2010. The Chicxulub Asteroid Impact and Mass Extinction at the Cretaceous-Paleogene Boundary. Science (80-.). 327, 1214–1218. https://doi.org/10.1126/science.1177265

Schultz, P. H., 1992. Atmospheric effects on ejecta emplacement and crater formation on Venus from Magellan. Journal of Geophysical Research: Planets, 97(E10), 16183-16248.

Schultz, P.H., Gault, D.E., 1990. Prolonged global catastrophes from oblique impacts. Spec. Pap. Geol. Soc. Am. 247, 239–261. https://doi.org/10.1130/SPE247-p239

Schultz, P.H., Quintana, S.N., 2017. Impact-generated winds on Mars. Icarus 292, 86–101. https://doi.org/10.1016/j.icarus.2017.03.029

Schwarz, W.H., Trieloff, M., Bollinger, K., Gantert, N., Fernandes, V.A., Meyer, H.P., Povenmire, H., Jessberger, E.K., Guglielmino, M., Koeberl, C., 2016. Coeval ages of Australasian, Central American and Western Canadian tektites reveal multiple impacts 790 ka ago. Geochim. Cosmochim. Acta 178, 307–319.

https://doi.org/10.1016/j.gca.2015.12.037

Shimo, Y., Nishimura, C., G., C., Matsumoto, T., Zhong, F., Yokoyama, T., Nakajima, S., Matsuda, J., 2010. Noble gas compositions and water contents in tektites from Hainan Island. Chikyukagaku (Geochemistry) 44, 43–50.

Sieh, K., Herrin, J., Jicha, B., Angel, D.S., Moore, J.D.P., Banerjee, P., Wiwegwin, W., Sihavong, V., Singer, B., Chualaowanich, T., Charusiri, P., 2019. Australasian impact crater buried under the Bolaven volcanic field, Southern Laos. Proc. Natl. Acad. Sci. U. S. A. 117, 1346–1353. https://doi.org/10.1073/pnas.1904368116

Songtham, W., Duangkrayom, J., Jintasakul, P., 2012. An Australasian Tektite from the Yasothon Soil Series, Noen Sa-nga, Chaiyaphum, Northeastern Thailand. Acta Geosci. Sin. 33, 59–64. https://doi.org/10.3975/cagsb.2012.s1.28

Songtham, W., Mildenhall, D.C., Jintasakul, P., Duangkrayom, J., 2011. Evidence of Sedimentary Deposits Generated by an Early Pleistocene Meteor Impact in Northeastern Thailand, in: International Conference on Geology, Geotechnology and Mineral Resources of Indochina (GEOINDO 2011).

Stauffer, M.R., Butler, S.L., 2010. The Shapes of Splash-Form Tektites: Their Geometrical Analysis, Classification and Mechanics of Formation. Earth, Moon Planets 107, 169–196. https://doi.org/10.1007/s11038-010-9359-y

Stöffler, D., 1972. Deformation and transformation of rock-forming minerals by natural and experimental shock processes. Fortschritte der Mineral. 49, 50–113.

Stöffler, D., Gault, D.E., Wedekind, J., Polkowski, G., 1975. Experimental hypervelocity impact into quartz sand: Distribution and shock metamorphism of ejecta. J. Geophys. Res. 80, 4062–4077. https://doi.org/10.1029/jb080i029p04062

Stöffler, D., Hamann, C., Metzler, K., 2018. Shock metamorphism of planetary silicate rocks and sediments: Proposal for an updated classification system. Meteorit. Planet. Sci. 53, 5–49. https://doi.org/10.1111/maps.12912

Stöffler, D., Langenhorst, F., 1994. Shock metamorphism of quartz in nature and experiment: I. Basic observation and theory. Meteoritics 29, 155–181.

Sturm, S., Wulf, G., Jung, D., Kenkmann, T., 2013. The ries impact, a double-layer rampart crater on earth. Geology 41, 531–534. https://doi.org/10.1130/G33934.1

Surenian, R., 1988. Scanning electron microscope study of shock features in pumice and gneiss from köfels (Tyrol, Austria). Geol. Paläont. Mitt. Innsbruck 15, 135–143.

Tada, R., Sato, S., Irino, T., Matsui, H., Kennett, J.P., 2000. Millennial-scale

compositional variations in late Quaternary sediments at site 1017, Southern California. Proc. Ocean Drill. Progr. Sci. Results 167, 277–296. https://doi.org/10.2973/odp.proc.sr.167.222.2000

Tada, R., Tada, T., Yoshioka, J., 2020. Discovery of Australasian microtektites in the hemipelagic sediments of the Japan Sea: It' s significance and implications. Abstr. JpGU-AGU Jt. Meet. 2020 MIS04-P01, 2020.

Tada, T., Tada, R., Chansom, P., Songtham, W., Carling, P. A., Tajika, E., 2020. In situ occurrence of Muong Nong-type Australasian tektite fragments from the Quaternary deposits near Huai Om, northeastern Thailand. Progress in Earth and Planetary Science, 7(1), 1-15.

Takagi, Y., Mizutani, H., Kawakami, S.I., 1984. Impact fragmentation experiments of basalts and pyrophyllites. Icarus 59, 462–477. https://doi.org/10.1016/0019-1035(84)90114-3

Takashimizu, Y., Iiyoshi, M., 2016. New parameter of roundness R: circularity corrected by aspect ratio. Prog. Earth Planet. Sci. 3, 2. https://doi.org/10.1186/s40645-015-0078-x

Tamura, T., 1992. Landform Development and Related Environmental Changes in the Chi River Basin, Northest Thailand. Sci. REPORTS TOHOKU Univ. 7TH Ser. 42, 107–127.

Teraoka, Y., Okumura, K., 2011. The Geological Map of Asia,(at 1:5,000,000 scale).

Turcotte, L.D., 1986. Fractals and Fragmentation. J. Geophys. Res. 91, 1921–1926.

Twiss, R.J., 1974. Structure and significance of planar deformation features in synthetic quartz. Geology 2, 329–332. https://doi.org/10.1130/0091-7613(1974)2<329:SASOPD>2.0.CO;2

Van Hoesel, A., Hoek, W.Z., Pennock, G.M., Kaiser, K., Plümper, O., Jankowski, M., Hamers, M.F., Schlaak, N., Küster, M., Andronikov, A. V., Drury, M.R., 2015. A search for shocked quartz grains in the Allerød-Younger Dryas boundary layer. Meteorit. Planet. Sci. 50, 483–498. https://doi.org/10.1111/maps.12435

Vernooij, M.G.C., Langenhorst, F., 2005. Experimental reproduction of tectonic deformation lamellae in quartz and comparison to shock-induced planar deformation features. Meteorit. Planet. Sci. 40, 1353–1361. https://doi.org/10.1111/j.1945-5100.2005.tb00406.x

Vilayhack, S., Duangsurigna, S., Phomkenthao, S., Voravong, A., Vilaysan, P.,

Khounchanthida, T., Phommakaysone, K., Goto, M., Negishi, Y., Tsuda, K., Watanabe, Y., 2008. Geology of the Attapu district. With Geological Sheet Map (D-48-XII) at 1:200,000.

Vrana, S., 1987. TheŠevĚtín Astrobleme, southern Bohemia, Czechoslovakia. Geol. Rundschau 76, 505–528.

Walter, L.S., 1965. Coesite discovered in tektites. Science (80-.). 147, 1029–1032. https://doi.org/10.1126/science.147.3661.1029

Wasson, J.T., 1991. Layered tektites: a multiple impact origin for the Australasian tektites. Earth Planet. Sci. Lett. 102, 95–109. https://doi.org/10.1016/0012-821X(91)90001-X

Wasson, J.T., Pitakpaivan, K., Putthapiban, P., Salyapongse, S., Thaothimthong, B., McHone, J.F., 1995. Field recovery of layered tektites in northeast Thailand. J. Geophys. Res. 100, 14383–14389.

White, S., 1973. Deformation Lamellae in Naturally Deformed Quartz. Nat. Phys. Sci. 245, 26–28. https://doi.org/10.1038/246421a0

Wongsomsak, S., 1986. Salinization in Northeast Thailand. Southeast Asian Stud. 24, 133–153.

Xu, Y., 2018. The fractal evolution of particle fragmentation under different fracture energy. Powder Technol. 323, 337–345. https://doi.org/10.1016/j.powtec.2017.10.011

Yamei, H., Potts, R., Baoyin, Y., Zhengtang, G., Deino, A., Wei, W., Clark, J., Guangmao, X., Weiwen, H., 2000. Mid-Pleistocene Acheulan-like Stone Technology of the Bose Basin, South China. Science (80-.). 287, 1622–1626. https://doi.org/10.1126/science.287.5458.1622

Appendix

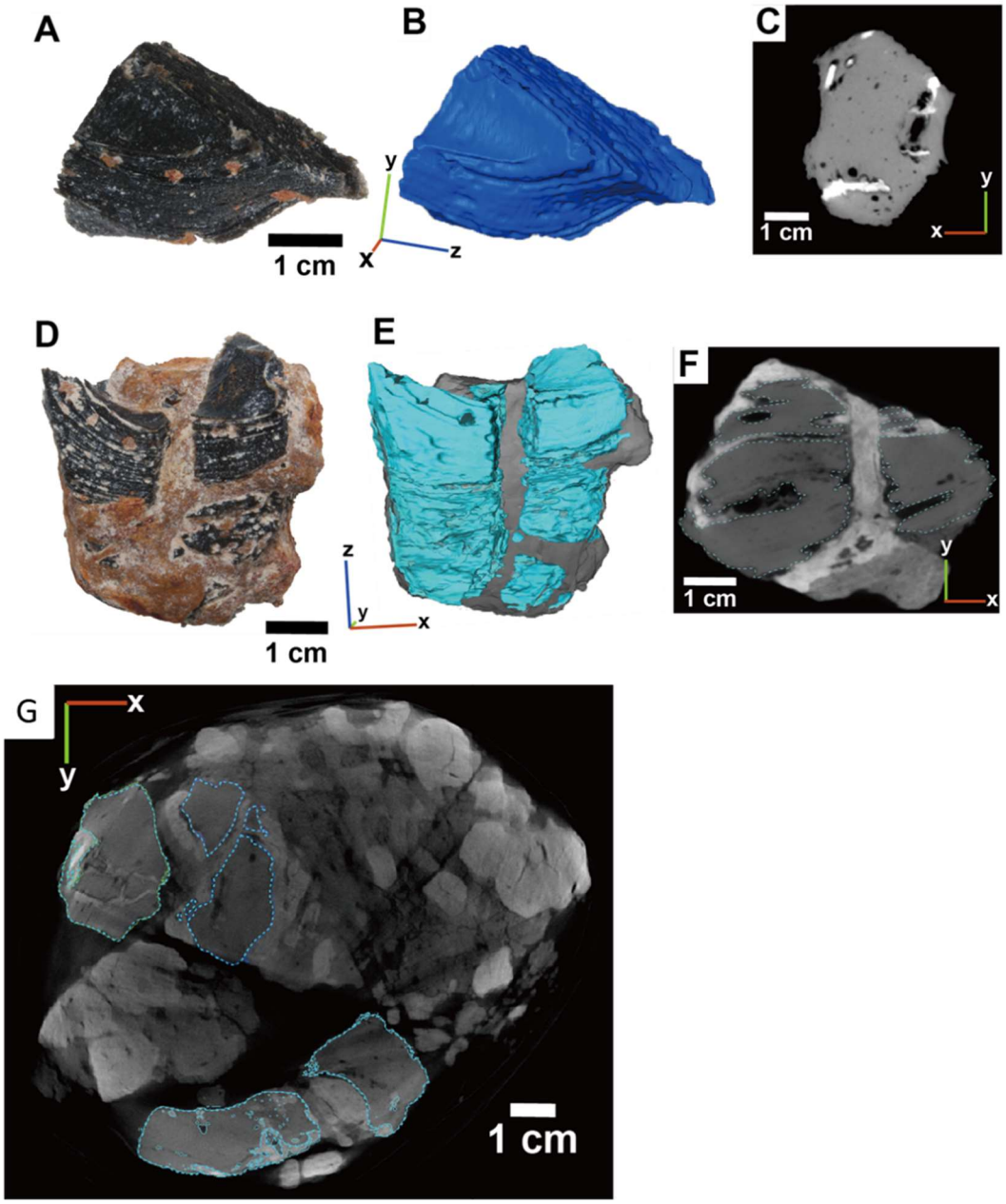

Figure A1.1 Examples of the CT scan 3D imaging of the MN tektite fragments. A-C) Sample HO06MN33, D-E) Sample HO06MN163a-e (five pieces are cohered with matrix). A, D) Photograph of the samples. B, E) Results of 3D imaging of the samples. C, F) Examples of CT scan cross-sections. The tektite fragments appear on the cross-sections as the angular shaped areas that are moderate gray color, homogeneous, and has elongated vesicles. G) the example of the CT cross-section of the block sample. Tektite fragments that appear in the cross-section are entrained with the dashed lines.

Table A1.1 Weight and size of the MN tektite fragments from the HO06 section

Sample No.	weight (g)	long axis a (cm)	medium axis b (cm)	short axis c (cm)	memo
HO06MN 1	1.1121	17.40	12.50	9.90	
HO06MN 2	1.1445	20.90	14.30	4.40	
HO06MN 3	0.0962	n.a.	n.a.	n.a.	used for thin section observation
HO06MN 4	0.6311	18.00	14.65	5.55	
HO06MN 5	10.1491	29.25	19.50	13.00	
HO06MN 6	7.3895	38.00	18.65	10.65	
HO06MN 7	0.5779	n.a.	n.a.	n.a.	used for thin section observation
HO06MN 8	1.2458	n.a.	n.a.	n.a.	used for thin section observation
HO06MN 9	3.3033	26.00	22.00	7.75	
HO06MN 10	0.7803	21.60	14.40	4.10	
HO06MN 11	1.6545	27.85	13.00	6.00	
HO06MN 12	1.8951	n.a.	n.a.	n.a.	used for thin section observation
HO06MN 13	2.8643	32.45	23.65	5.00	
HO06MN 14	0.7711	n.a.	n.a.	n.a.	used for thin section observation
HO06MN 15	2.0217	21.65	15.00	10.25	
HO06MN 16	1.0706	n.a.	n.a.	n.a.	used for EPMA analysis
HO06MN 17	0.9555	14.50	11.50	7.10	
HO06MN 18	0.7220	14.00	13.65	8.60	
HO06MN 19	0.0272	7.65	3.55	1.65	
HO06MN 20	1.0411	n.a.	n.a.	n.a.	used for EPMA analysis
HO06MN 21	1.1327	16.60	14.65	7.00	
HO06MN 22	0.9687	n.a.	n.a.	n.a.	used for EPMA analysis
HO06MN 23	0.0445	10.90	4.00	1.60	
HO06MN 24	11.3531	33.50	25.70	21.80	
HO06MN 25	0.3216	13.50	12.85	6.45	
HO06MN 26	8.2426	29.10	19.75	15.80	
HO06MN 27	10.6310	30.30	29.00	16.60	
HO06MN 28	4.2579	33.00	13.85	12.05	
HO06MN 29	12.1602	46.15	23.90	15.15	
HO06MN 30	22.2462	41.00	29.70	22.90	
HO06MN 31	33.3381	41.50	40.00	30.80	
HO06MN 32	11.9068	35.80	32.90	11.50	
HO06MN 32b	3.5536	25.60	18.05	8.00	
HO06MN 33	17.2784	39.25	28.05	21.40	
HO06MN 34	13.5215	36.15	34.75	22.45	
HO06MN 35	19.3375	38.00	32.40	12.00	
HO06MN 36	1.5243	20.20	10.05	8.55	
HO06MN 37	1.2681	19.90	12.35	6.25	
HO06MN 38	0.2097	16.20	8.00	6.20	
HO06MN 39	1.3996	26.70	20.00	9.20	
HO06MN 40	0.5640	23.25	13.35	8.80	
HO06MN 41a	0.1186	7.20	6.80	3.85	
HO06MN 41b	0.0285	7.10	3.90	2.35	
HO06MN 43a	0.1800	11.90	6.55	4.40	
HO06MN 43b	0.0072	4.15	2.35	1.20	
HO06MN 43c	0.0075	2.00	2.00	1.90	
HO06MN 44	1.3833	15.80	12.15	8.90	
HO06MN 45	2.1602	n.a.	n.a.	n.a.	used for thin section observation
HO06MN 46	7.3313	30.00	21.50	20.15	
HO06MN 47	3.4782	25.35	16.25	8.70	
HO06MN 48	8.1742	32.90	23.90	17.40	
HO06MN 49	0.2247	10.90	6.90	3.80	
HO06MN 50	3.4388	27.40	20.85	9.00	

Table A1.1 (continued)

HO06MN 51	0.0555	6.60	4.40	3.10	
HO06MN 52	0.0347	6.10	5.25	2.50	
HO06MN 53	0.1790	8.80	8.00	5.00	
HO06MN 54	0.1906	14.95	9.20	4.15	
HO06MN 55	0.0800	13.10	3.95	2.80	
HO06MN 56	0.2572	16.70	5.15	4.10	
HO06MN 57	0.1202	12.45	7.65	2.50	
HO06MN 58	0.0836	11.30	6.10	2.35	
HO06MN 59	0.0609	7.90	5.85	1.95	
HO06MN 60	0.0979	8.15	5.00	4.85	
HO06MN 61	0.0372	7.30	5.00	2.55	
HO06MN 62	0.0150	4.00	3.65	1.85	
HO06MN 63	0.0582	7.80	5.00	2.25	
HO06MN 64	0.0100	4.25	3.00	1.30	
HO06MN 65	0.1533	16.65	6.10	3.00	
HO06MN 66	0.0320	9.65	5.90	1.00	
HO06MN 67	0.1054	18.45	6.60	1.95	
HO06MN 68	0.4102	12.35	8.55	7.40	
HO06MN 69	0.0098	3.80	2.80	2.15	
HO06MN 70	0.0146	5.30	3.70	2.35	
HO06MN 71	0.0038	3.80	2.30	1.00	
HO06MN 72	0.0464	5.10	4.00	3.05	
HO06MN 73	0.0045	4.40	1.95	1.10	
HO06MN 74	0.0072	4.55	2.25	1.10	
HO06MN 75	0.1253	11.40	8.65	1.90	
HO06MN 76	0.0823	7.60	5.00	3.40	
HO06MN 77	3.1149	21.40	20.90	15.85	
HO06MN 78	1.0836	24.40	10.90	6.85	
HO06MN 88	1.4788	16.20	15.10	12.35	
HO06MN 80	0.5174	17.10	11.10	5.00	
HO06MN 81	0.0530	6.20	5.00	3.20	
HO06MN 82	0.4857	14.90	10.50	3.90	
HO06MN 83	0.9292	17.90	16.50	4.45	
HO06MN 84	1.5734	22.60	14.55	9.00	
HO06MN 85	1.4300	27.45	10.35	6.90	
HO06MN 86	1.4508	28.55	18.55	3.75	
HO06MN 87	0.1807	9.25	8.90	4.05	
HO06MN 79	0.5357	n.a.	n.a.	n.a.	used for EPMA analysis
HO06MN 89	0.3374	12.45	9.00	5.40	
HO06MN 90	1.3458	18.70	12.85	7.80	
HO06MN 91	4.3715	n.a.	n.a.	n.a.	used for thin section observation
HO06MN 92	0.3814	18.25	6.55	5.80	
HO06MN 93	0.5417	22.95	11.55	3.80	
HO06MN 94	1.8213	18.20	16.50	11.00	
HO06MN 95	1.7007	16.25	15.15	10.75	
HO06MN 96	2.0848	20.00	16.20	9.50	
HO06MN 97	3.5087	21.50	9.65	7.90	
HO06MN 98	1.0776	10.35	7.00	3.70	
HO06MN 99	0.9556	24.05	18.20	16.00	
HO06MN 101	3.7624	25.35	20.25	11.60	
HO06MN 102	1.7481	26.00	13.40	8.75	
HO06MN 103a	0.6658	12.00	11.00	6.10	
HO06MN 103b	0.1794	9.35	6.85	4.85	
HO06MN 103c	0.0583	7.55	7.00	3.00	

Table A1.1 (continued)

HO06MN 103d	0.1012	6.90	4.00	3.35
HO06MN 103e	0.0525	5.70	3.60	2.55
HO06MN 104	0.0989	4.30	3.30	2.90
HO06MN 105	1.7284	n.a.	n.a.	n.a. used for EPMA analysis
HO06MN 106a	1.0705	17.00	10.90	8.20
HO06MN 106b	0.9551	16.65	11.80	6.70
HO06MN 107	2.1685	26.45	12.20	12.00
HO06MN 108	3.4092	27.00	19.25	12.75
HO06MN 109	1.7090	20.50	18.10	7.40
HO06MN 111	0.7065	24.00	9.60	4.05
HO06MN 112	1.1888	n.a.	n.a.	n.a. used for thin section observation
HO06MN 113	0.6900	20.60	10.00	6.20
HO06MN 114	1.0682	16.30	15.10	7.15
HO06MN 115	0.2607	18.20	6.00	5.00
HO06MN 116	0.4724	15.80	11.50	4.15
HO06MN 117	0.2353	11.45	6.50	5.35
HO06MN 118	0.4574	12.40	9.50	6.60
HO06MN 119	0.4988	n.a.	n.a.	n.a. used for EPMA analysis
HO06MN 120	1.1961	23.25	12.35	7.85
HO06MN 121	0.6092	n.a.	n.a.	n.a. used for EPMA analysis
HO06MN 122	0.5340	n.a.	n.a.	n.a. used for EPMA analysis
HO06MN 123	0.3926	12.10	9.05	5.30
HO06MN 124	0.1480	n.a.	n.a.	n.a. used for EPMA analysis
HO06MN 125	0.0104	6.40	3.35	1.25
HO06MN 126	0.3452	11.45	10.45	5.60
HO06MN 127	0.2787	12.70	10.00	3.00
HO06MN 128	0.4720	15.10	9.00	5.25
HO06MN 129	0.7091	n.a.	n.a.	n.a. used for EPMA analysis
HO06MN 130	0.2982	14.10	8.90	4.85
HO06MN 131	0.5310	15.80	9.15	6.45
HO06MN 132	0.3424	13.10	8.15	6.30
HO06MN 133	0.2704	12.40	6.15	4.95
HO06MN 134	0.1474	9.75	7.15	4.00
HO06MN 135	0.1551	13.35	6.50	2.80
HO06MN 136	0.1768	12.95	5.50	3.90
HO06MN 137	0.2361	12.35	11.00	4.95
HO06MN 138	0.4431	13.30	8.00	6.90
HO06MN 139	0.1342	7.50	7.40	4.50
HO06MN 140	0.2261	11.80	10.35	3.80
HO06MN 141	0.3532	n.a.	n.a.	n.a. used for EPMA analysis
HO06MN 142	0.2818	n.a.	n.a.	n.a. used for thin section observation
HO06MN 143	0.2218	13.90	7.80	2.45
HO06MN 144	0.2838	11.50	9.45	4.40
HO06MN 145	0.0402	6.00	4.75	2.40
HO06MN 146	0.0632	7.55	4.15	2.65
HO06MN 147	0.1011	n.a.	n.a.	n.a. used for thin section observation
HO06MN 148	0.1362	15.35	5.25	3.70
HO06MN 149	0.1289	8.00	7.65	4.00
HO06MN 150	0.0637	8.05	4.35	3.45
HO06MN 151	0.0473	7.00	4.20	2.35
HO06MN 152	0.1015	10.05	6.70	2.25
HO06MN 153	0.1529	14.15	5.30	4.65
HO06MN 154	0.1101	9.20	5.50	4.65
HO06MN 155	0.1191	8.70	8.50	3.60

Table A1.1 (continued)

HO06MN 156	0.0682	8.60	6.80	2.40
HO06MN 157	0.0749	7.30	4.00	3.55
HO06MN 158	0.0430	8.00	5.00	2.30
HO06MN 159	0.0707	7.55	5.15	3.00
HO06MN 160	0.0294	9.60	2.95	1.70
HO06MN 161	0.0663	8.90	4.90	3.40
HO06MN 162	0.0351	7.45	4.75	2.00
HO06MN 163a	12.5100	38.84	24.79	23.10
HO06MN 163b	5.1207	24.56	18.04	13.35
HO06MN 163c	6.5316	24.49	20.88	16.94
HO06MN 163d	2.6571	19.74	14.29	14.06
HO06MN 163e	0.4050	9.94	8.23	6.37
HO06MN 164	18.7485	32.20	27.55	24.20
HO06MN 165	14.4278	36.80	35.55	19.00
HO06MN 166	13.2860	35.15	22.85	11.20
HO06MNBS 1-1	0.5441	17.05	8.55	4.85
HO06MNBS 1-2	0.6269	19.25	7.85	5.15
HO06MNBS 1-3	0.1945	13.10	6.55	3.45
HO06MNBS 1-4	0.2576	10.60	7.10	5.85
HO06MNBS 1-5	0.1678	10.00	5.85	4.40
HO06MNBS 1-6	0.1301	8.25	6.30	4.55
HO06MNBS 1-7	0.0960	9.50	5.85	2.60
HO06MNBS 1-13	0.0552	6.40	6.10	4.05
HO06MNBS 2-1	32.1720	52.80	39.50	19.85
HO06MNBS 2-2	5.1889	23.50	22.10	15.00
HO06MNBS 2-3	26.9820	41.55	33.05	21.00
HO06MNBS 2-4	33.2225	44.50	35.15	29.75
HO06MNBS 2-5	19.6052	38.00	32.45	18.70
HO06MNBS 2-6	7.8953	35.85	17.90	16.85
HO06MNBS 2-7	9.0149	30.45	23.35	17.60
HO06MNBS 2-8	3.6472	27.65	15.10	12.15
HO06MNBS 2-9	3.6228	24.40	15.00	14.95
HO06MNBS 2-10	3.4908	22.90	16.45	11.00
HO06MNBS 2-11	2.1709	18.90	14.75	9.40
HO06MNBS 2-12	2.3266	21.25	13.25	12.40
HO06MNBS 2-13	1.6038	17.10	13.70	11.00
HO06MNBS 2-14	1.5627	16.75	14.60	9.45
HO06MNBS 2-15	1.8966	16.85	14.55	11.10
HO06MNBS 2-16	1.2979	15.55	12.80	7.95
HO06MNBS 2-17	1.8120	14.90	13.55	12.05
HO06MNBS 2-18	1.3236	13.65	9.55	8.00
HO06MNBS 2-19	1.0571	15.85	12.10	9.95
HO06MNBS 2-20	0.8051	15.25	10.15	6.05
HO06MNBS 2-21	0.7660	18.45	8.60	7.50
HO06MNBS 2-22	0.6541	14.00	11.30	6.75
HO06MNBS 2-23	0.9148	14.30	11.15	10.25
HO06MNBS 2-24	0.8392	16.30	10.35	9.45
HO06MNBS 2-25	0.5125	17.00	10.65	4.80
HO06MNBS 2-26	0.5375	15.40	13.35	4.15
HO06MNBS 2-27	0.5204	15.15	10.55	5.10
HO06MNBS 2-28	0.5586	16.20	9.65	5.90
HO06MNBS 2-29	0.3638	10.60	10.25	6.30
HO06MNBS 2-30	0.4000	13.10	10.10	7.10
HO06MNBS 2-31	0.1277	12.25	7.90	2.70

Table A1.1 (continued)

HO06MNBS 2-32	0.3924	9.60	9.45	5.95
HO06MNBS 2-33	0.1910	10.50	6.95	5.20
HO06MNBS 2-34	0.0747	11.45	5.85	2.85
HO06MNBS 2-35	0.1138	9.55	5.15	3.20
HO06MNBS 2-36	0.1248	8.30	7.30	3.40
HO06MNBS 2-37	0.1365	11.95	6.35	3.35
HO06MNBS 2-38	0.1353	12.55	6.20	3.75
HO06MNBS 2-39	0.1729	9.30	5.90	4.60
HO06MNBS 2-40	0.3149	13.50	6.95	4.90
HO06MNBS 2-41	0.4016	10.90	10.35	7.25
HO06MNBS 2-42	0.3093	17.45	6.70	4.60
HO06MNBS 2-45	0.1768	10.95	10.55	3.15
HO06MNBS 2-46	0.1213	18.15	4.10	3.20
HO06MNBS 2-47	0.2138	14.30	6.70	4.40
HO06MNBS 2-48	0.1455	10.85	7.25	2.85
HO06MNBS 2-49	0.3974	14.45	9.95	3.90
HO06MNBS 2-50	0.2076	12.00	8.80	3.95
HO06MNBS 2-51	0.0756	17.00	4.05	2.90
HO06MNBS 2-52	0.0515	8.80	4.35	3.40
HO06MNBS 2-53	0.1771	10.10	6.40	4.30
HO06MNBS 2-54	0.2008	10.60	7.40	4.65
HO06MNBS 2-55	0.1430	9.20	6.40	6.10
HO06MNBS 2-56	0.0928	11.85	5.20	4.10
HO06MNBS 2-57	0.2013	10.75	8.20	4.10
HO06MNBS 2-58	0.1136	9.20	7.95	3.20
HO06MNBS 2-60	0.0765	9.05	4.15	3.35
HO06MNBS 2-64	0.0952	7.70	7.30	3.10
HO06MNBS 2-66	0.0683	7.55	5.30	3.20
HO06MNBS 2-67	0.0564	13.50	4.15	2.60
HO06MNBS 2-68	0.1146	13.40	5.90	3.80
HO06MNBS 2-73	0.0891	8.40	5.90	3.80
HO06MNBS 2-74	0.1000	11.00	7.55	1.80
HO06MNBS 2-77	0.0474	8.00	4.95	3.30
HO06MNBS 2-78	0.0717	9.75	5.15	3.40
HO06MNBS 2-89	0.0594	6.10	5.50	3.95
HO06MNBS 2-90	0.1075	7.95	7.60	3.90
HO06MNBS 4-1	17.2205	35.60	31.50	25.50
HO06MNBS 4-2	12.9954	34.00	30.70	19.00
HO06MNBS 4-3	6.2799	28.55	24.10	17.15
HO06MNBS 4-4	4.1438	30.65	18.00	11.85
HO06MNBS 4-5	1.8845	28.40	13.20	7.20
HO06MNBS 4-6	4.1036	21.60	12.30	11.45
HO06MNBS 4-7	5.1606	24.45	17.40	16.40
HO06MNBS 4-8	2.4351	19.55	13.00	12.45
HO06MNBS 4-9	0.3906	13.65	9.00	5.00
HO06MNBS 4-10	0.7250	14.15	9.15	7.10
HO06MNBS 4-11	0.2971	13.70	7.70	3.30
HO06MNBS 4-12	0.1704	10.00	7.50	2.85
HO06MNBS 4-13	0.1832	9.50	7.45	4.65
HO06MNBS 4-14	0.1775	9.60	7.40	4.85
HO06MNBS 4-15	0.1088	8.10	5.05	4.00
HO06MNBS 4-16	0.2020	10.65	6.60	5.25
HO06MNBS 4-19	0.0856	8.45	5.15	3.20
HO06MNBS 4-22	0.1286	10.00	4.90	5.00

Table A1.1 (continued)

HO06MNBS 4-23	0.1114	7.50	6.35	5.60
HO06MNBS 4-24	0.1414	12.30	5.90	2.70
HO06MNBS 4-26	0.1160	9.60	6.00	4.25
HO06MNBS 5-1	28.8536	37.60	31.10	29.10
HO06MNBS 5-2	8.9768	31.45	20.80	9.40
HO06MNBS 5-3	3.3329	26.30	15.65	13.00
HO06MNBS 5-4	3.0346	28.10	18.90	11.35
HO06MNBS 5-5	1.3892	17.40	16.55	11.05
HO06MNBS 5-6	2.3466	20.20	14.00	11.25
HO06MNBS 5-7	2.1890	20.15	15.55	9.60
HO06MNBS 5-8	1.5041	18.25	11.25	10.65
HO06MNBS 5-9	1.3690	16.70	13.65	7.85
HO06MNBS 5-10	1.2095	19.80	11.00	7.40
HO06MNBS 5-11	1.2399	17.95	13.50	7.30
HO06MNBS 5-12	1.8751	16.15	12.95	12.50
HO06MNBS 5-13	1.0685	16.65	13.55	9.90
HO06MNBS 5-14	0.9983	17.85	11.30	11.00
HO06MNBS 5-15	0.7372	15.00	10.20	9.00
HO06MNBS 5-16	0.5182	12.05	9.30	8.60
HO06MNBS 5-17	0.6124	14.00	13.55	4.45
HO06MNBS 5-18	0.3736	12.00	7.15	6.00
HO06MNBS 5-19	0.2176	13.15	6.20	4.85
HO06MNBS 5-20	0.1252	12.60	7.30	3.15
HO06MNBS 5-21	0.1486	11.60	7.30	2.90
HO06MNBS 5-22	0.3943	10.95	8.70	6.30
HO06MNBS 5-23	0.1800	9.50	7.50	5.20
HO06MNBS 5-24	0.1629	9.00	8.00	4.95
HO06MNBS 5-25	0.1698	12.25	5.40	5.05
HO06MNBS 5-27	0.1691	9.75	7.45	5.20
HO06MNBS 5-28	0.1132	10.10	7.85	3.30
HO06MNBS 5-35	0.0667	9.00	6.00	2.45
HO06MNBS 5-36	0.0954	10.85	5.70	3.35
HO06MNBS 5-37	0.0573	7.00	6.35	2.95
HO06MNBS 6-1	3.0408	21.20	18.65	9.15
HO06MNBS 6-2	13.0017	29.70	28.50	21.80
HO06MNBS 6-3	5.8095	26.40	23.05	18.00
HO06MNBS 6-4	5.8858	24.50	19.90	17.20
HO06MNBS 6-5	3.6547	28.65	19.00	8.55
HO06MNBS 6-6	6.8756	23.90	18.40	17.40
HO06MNBS 6-7	3.5534	27.85	21.30	20.50
HO06MNBS 6-8	4.9811	25.40	19.25	11.35
HO06MNBS 6-9	0.7015	13.25	11.25	6.60
HO06MNBS 6-10	1.6030	25.70	14.00	7.65
HO06MNBS 6-11	0.3918	22.45	8.05	4.65
HO06MNBS 6-12	0.4822	15.85	9.40	5.05
HO06MNBS 6-13	0.6453	11.35	10.40	7.35
HO06MNBS 6-14	0.3088	18.45	8.05	3.40
HO06MNBS 6-15	0.4124	18.80	8.70	3.25
HO06MNBS 6-16	0.3207	9.95	8.45	5.75
HO06MNBS 6-17	0.4223	15.40	11.10	4.75
HO06MNBS 6-18	0.2731	13.60	6.20	4.60
HO06MNBS 6-19	0.3170	13.75	7.55	4.00
HO06MNBS 6-20	0.2817	8.05	7.30	5.90
HO06MNBS 6-21	0.1239	8.80	6.55	3.00

Table A1.1 (continued)

HO06MNBS 6-22	0.1598	10.35	7.00	4.00
HO06MNBS 6-23	0.1694	9.20	8.85	4.10
HO06MNBS 6-24	0.2669	11.55	6.60	4.80
HO06MNBS 6-25	0.0873	8.30	6.75	2.80
HO06MNBS 6-26	0.1635	9.45	6.40	4.35
HO06MNBS 6-27	0.0788	8.10	7.00	2.45
HO06MNBS 6-28	0.1056	13.15	5.40	2.95
HO06MNBS 6-37	0.0686	8.55	6.20	3.20

Figure A2.1 – Figure A3.35 are not available for publication because it is scheduled to be published in a journal within five years.
本章については、5 年以内に雑誌等で刊行予定のため、非公開